FISSION PRODUCT DATA FOR THERMAL REACTORS

Part I
A Data Set for EPRI-CINDER Using ENDF/B-IV

EPRI NP-356
(Research Project 453)
(ERDA E(29-2)-3608)

Final Report

December 1976

Prepared by

Los Alamos Scientific Laboratory
Theoretical Division
UNIVERSITY OF CALIFORNIA
Los Alamos, New Mexico 87545

PRINCIPAL INVESTIGATORS
T. R. England
W. B. Wilson
M. G. Stamatelatos

PROGRAM MANAGER
P. G. Young

Prepared for

Electric Power Research Institute
3412 Hillview Avenue
Palo Alto, California 94304

and

Energy Research and Development Administration
20 Massachusetts Avenue
Washington, D. C. 20545

EPRI Project Manager
O. Ozer

ERDA Representative
P. B. Hemmig

ABSTRACT

A four-group fission-product neutron absorption library, appropriate for use in thermal reactors, is described. All decay parameters are taken from ENDF/B-IV. The absorption cross sections are also processed from ENDF/B-IV files, first into a 154-group set and subsequently collapsed into the 4-group set described in this report. The decay and cross section data were used to form 84 linear chains in the CINDER code format. These chains contain all significant fission products having half-lives exceeding 4 hours -- a total of 186 nuclides. A 12-chain set containing one pseudo-chain for use in spatial depletion calculations is described. This set accurately reproduces the aggregate absorption buildup of the 84 chains. Part 1 of this report describes the chains and processed data, results of comparison calculations for various fuels, and a comparison of calculated temporal fission-product absorption buildup with corresponding results from a long-term fuel irradiation and cooling integral experiment. Part 2 is a self-contained users manual for a modified version of the basic CINDER code (EPRI-CINDER) including a detailed chain description, data libraries, input formats, typical output, and a code listing.

ACKNOWLEDGMENTS

The authors gratefully acknowledge the assistance of R. E. MacFarlane in providing modifications to the NJOY code required for processing the abbreviated ENDF/B-IV fission-product cross section files. We appreciate the efforts of N. L. Whittemore in maintaining and updating the many versions of the libraries and performing the computer calculations. We are grateful to B. G. Atencio and S. L. Carlson for their tedious artwork in producing the illustrations and to C. I. Baxman for typing the manuscript.

CONTENTS

FIGURES

TABLES

SUMMARY

The rate of production and buildup of various fission product nuclides during the operation of a power reactor must be known accurately in order to optimize the utilization of nuclear fuel. Information about the heat generated during the radioactive decay of such nuclides is also required for loss of coolant and safety analyses. In view of this need, the Fission Product Subcommittee of the Cross Section Evaluation Working Group (responsible for the development of the national reference nuclear data base - ENDF/B) has recently prepared, primarily under ERDA funding, a massive data file containing information for over eight hundred fission product nuclides. The principal investigators for the present project have been major contributors to the development of this file which has been released as part of the fourth version of ENDF/B.

The objective of the present project has been the reduction of this major data base into a form more appropriate for use in thermal reactor core analysis and burnup calculations. This has been accomplished by grouping the fission product nuclides into 84 linearized decay chains and calculating the effective fission yields and four energy group cross sections for the most important, longer lived nuclides in each chain. As a further simplification, a second set consisting of 11 major decay chains and a twelfth "fictitious" chain accounting for the remaining nuclides has also been prepared. The resulting libraries are given in a form that can be used directly in the computer code CINDER. This code is widely used for LWR burnup calculations and it constitutes an integral part of the EPRI-CELL module of EPRI's fuel cycle analysis code system ARMP. An upgraded version of the code (renamed EPRI-CINDER) has also been produced as part of this project. At present the libraries can be used in EPRI-CINDER or earlier versions of the code in a stand-alone move. Incorporation into ARMP is being considered as a topic for a future report.

The description of the work carried out under the present contract (RP453) is given in two separate and self-contained parts:

- Part I gives a description of the procedures followed in reducing, processing and testing of the basic data.
- Part II is a users manual for EPRI-CINDER.

Complete listings of the libraries and the code EPRI-CINDER are given in appendices to Part II. Because the libraries may be of interest to persons unfamiliar with the CINDER input formalism, a quick key to the listings is also given in the project managers introduction to Part II.

Odelli Ozer
EPRI Project Manager

Section 1
INTRODUCTION

The temporal concentrations of fission-product nuclei produced in a nuclear reactor are described by a large set of coupled differential equations, each nuclide concentration being determined by a history of gains from direct fission yield, transmutation and radioactive decay from parent nuclei, and losses from its own decay and particle absorption. In 1962 the depletion and fission-product computer program CINDER[1] was published. It simplified the solution for fission-product concentrations by resolving the complicated nuclide couplings into "linear chains." Each linear chain represents a unique linear path from nuclide to nuclide, resulting in small independent sets of coupled differential equations describing the rate of change of "partial concentrations" of nuclides in each chain. The solution of a large set of coupled differential equations was thus reduced to the solution of a number of small sets of coupled differential equations, each characterized by a single generalized form. Because of the linear nature of the chain (a result of the Markov process), the generalized equations may be solved sequentially for the partial concentration of each nuclide in the chain. Nuclide concentrations are then obtained by summing partial concentrations. The mathematical aspects of the linearization technique used in the EPRI-CINDER code, a modification of the original code, are examined in the following section.

In order to maintain compatibility with the original code and supplemental user-developed data, EPRI-CINDER does not offer some features (e.g., free form input format) present in other recent versions[2] of the code. Input data for EPRI-CINDER must carefully follow the specified order and format typical of the original code. Details on the input format and data libraries of EPRI-CINDER, as well as its improvements over the original code, are deferred to Part 2 of this report. Part 2 is a self-contained users manual for the code and associated data libraries; Part 1 describes the development of the libraries, survey calculations, and data testing results.

The data set used with EPRI-CINDER must necessarily reflect a unique selection of linear chains and include pertinent cross-section, decay, branching, and fission-yield data. The data set[3] released for use with the original

code used 67 linear chains to describe 163 fission-product nuclides. A subsequent and more widely used data set[4] used 69 linear chains to describe 179 fission-product nuclides. These data sets, representing the most comprehensive accumulation of fission-product data to the dates of their release, were generally limited to nuclear data published during or prior to 1965 and included assumptions on the energy dependence of cross sections in the absence of reliable data. A later version, updating the 1965 library through 1971, showed only minor differences in aggregate absorptions and was, therefore, not published.

In 1974 the Fission-Product Subcommittee Task Force of the Cross Section Evaluation Working Group (CSEWG) completed and released through the National Neutron Cross Section Center of the Brookhaven National Laboratory (BNL) a comprehensive library of fission-product data. This library is known as the version four Evaluated Nuclear Data File (ENDF/B-IV) fission-product data library. The Nuclear Data Group T-2 of the Los Alamos Scientific Laboratory (LASL), under contract with the Electric Power Research Institute (EPRI), has produced a new data set for EPRI-CINDER using data processed from this library.

The production of this new 84-chain data set and its companion 12-chain reduced set are described in the following sections of this report. The 84-chain set includes all significant fission-product nuclides having half-lives in excess of 4 hours. Its primary use will be for calculations of neutron absorption buildup and long-lived radioactive nuclide concentrations pertinent to radiological hazards studies. The 12-chain set is convenient for use in spatial depletion codes; it accurately approximates the aggregate fission-product absorption buildup, including transient absorption properties of the 84-chain set.

Section 2
THEORY

Nuclide Coupling

Before investigating the mathematical treatment of fission-product nuclide concentrations, we might first recall the parameters pertinent to the description of fission products in a reactor environment. The magnitude of the problem is illustrated in Fig. 1, which displays the properties governing the coupling of fission-product nuclei in the small range $84 \leqslant A \leqslant 88$.

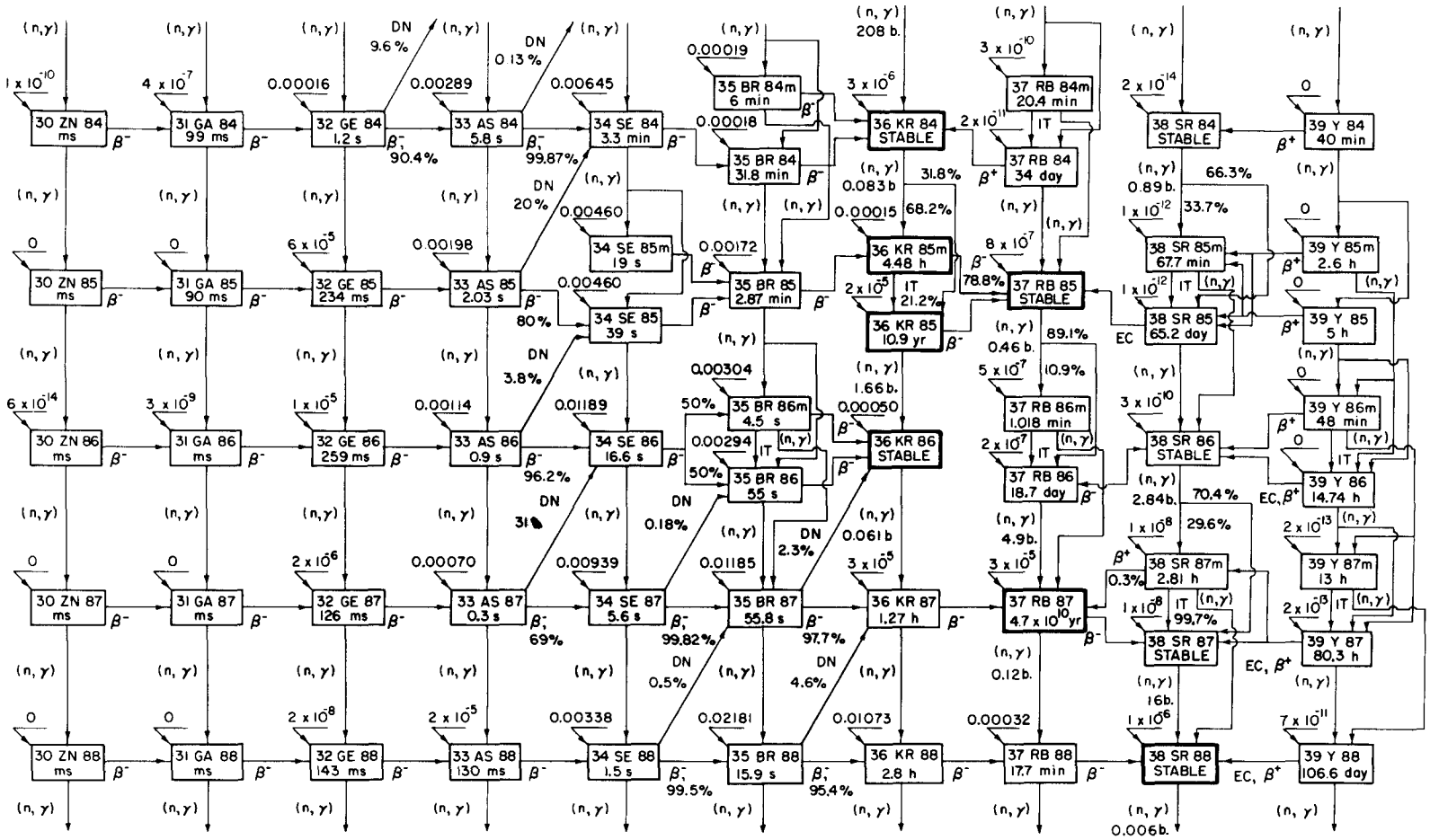

Fig. 1. Fission Products, $84 \leq A \leq 8$

Fission fragments are distributed in mass according to the familiar "double-humped" mass distribution curve. The fission yield to a particular mass is generally concentrated among a very few isobars well below the line of stability. These low-Z, neutron-rich nuclei are typically short lived, and the fission products of each mass migrate via β^- decay toward the more stable nuclei. Direct fission yield fractions to the stable or long-lived nuclides are small. The high-Z, proton-rich nuclei generally decay by β^+ emission or electron capture and receive little or no direct yield.

Competing with the normal scheme of radioactive decay is the transformation of nuclides to high-mass chains by neutron absorption. Indeed, it seems quite conceivable that, in a suitably large neutron flux of long duration, a light nucleus originating as a fragment of fission (e.g., $^{70}_{27}Co$) may, through a sequence of decay and transmutation, be transformed into a heavy nucleus (e.g., $^{186}_{74}W$). Adding isomeric levels and their associated decay and absorption branching, the avenues to and from a particular nucleus may be numerous.

Since we are interested here in the temporal description of neutron absorbers, we are permitted a number of simplifications. The low-Z isobars below the line of stability are typically very short lived. In the environment of an operating reactor, these nuclei rapidly reach low equilibrium concentrations having negligible macroscopic absorption and transient absorption properties. We consider these nuclei to β^- decay instantaneously to the next isobars of higher atomic number or, in the case of short-lived isomers, to γ-decay to ground states or β^--decay to the next isobar, as determined by branching fractions. The same treatment may be applied to daughter nuclei having longer, yet still limited, longevity.

We can easily justify ignoring transmutation via neutron absorption by these short-lived nuclei by simply comparing decay and absorption rates, using liberal flux and cross-section estimates. We can also ignore delayed neutron (β^-n) decay to the lower masses for reasons noted in Sec. 3.

Short-lived, neutron-rich nuclei may be assumed to instantaneously decay by β^- emission or isomeric transition until a "long-lived" nuclide is produced for which we must evaluate the temporal impact of its own macroscopic absorption or transient effect on that of its daughter(s). One could not, for example, neglect the 6.565 h half-life of $^{135}_{53}I$, precursor of $^{135}_{54}Xe$, which leads

to the familiar xenon transient. *We have chosen four hours as the limiting half-life value, consistently assuming shorter-lived, low-Z isobars to transpire upon birth and assigning their cumulative yield to the first daughter(s) with half-lives exceeding four hours.*

Because of their low yield, high-Z isobars appear in only trace concentrations and account for very little of the macroscopic absorption buildup of the fission-product ensemble. Depending upon their stability and yield, these nuclei may either be assumed to β^+ decay instantaneously or be ignored altogether.

Using the above simplifications relative to radioactive decay, the problem of describing absorption buildup is greatly reduced. Of the 56 nuclei in Fig. 1 that may realistically be considered to have non-zero concentrations in a reactor environment, only the 7 nuclei boldly marked need be considered in accurately describing the temporal macroscopic absorption properties of fission products in the given mass range.

Further simplifications may be made after examining the neutron absorption couplings. Again, using a liberal flux estimate, the sources of $^{85m}_{36}Kr$ and $^{85}_{36}Kr$ from $^{84}_{36}Kr$ radiative capture are found to be negligable in comparison to that resulting from fission yield. The same argument may be applied to the weak couplings of $^{85m}_{36}Kr$ to $^{86}_{36}Kr$, $^{86}_{36}Kr$ to $^{87}_{37}Rb$, and $^{88}_{38}Sr$ to $^{89}_{38}Sr$. Though these weak couplings may be ignored as sources to product nuclei, we will include the associated losses in describing the absorbers. The complicated schematic of Fig. 1 can now, for our purpose, be replaced by the simplified scheme of Fig. 2(a).

It should be noted here that $^{84}_{36}Kr$ is coupled to lighter nuclei not shown. Also, two clusters of nuclei have been isolated, each cluster being independent of all other fission-product concentrations. This is not a general property of fission products, for there is generally strong coupling from mass to mass.

The yield values corresponding to the nuclides explicitly included in the chain structure must reflect the simplifications previously described. For example, the effective fission yield fraction now associated with $^{84}_{36}Kr$ is composed of its cumulative yield (i.e., the sum of its direct fission-yield

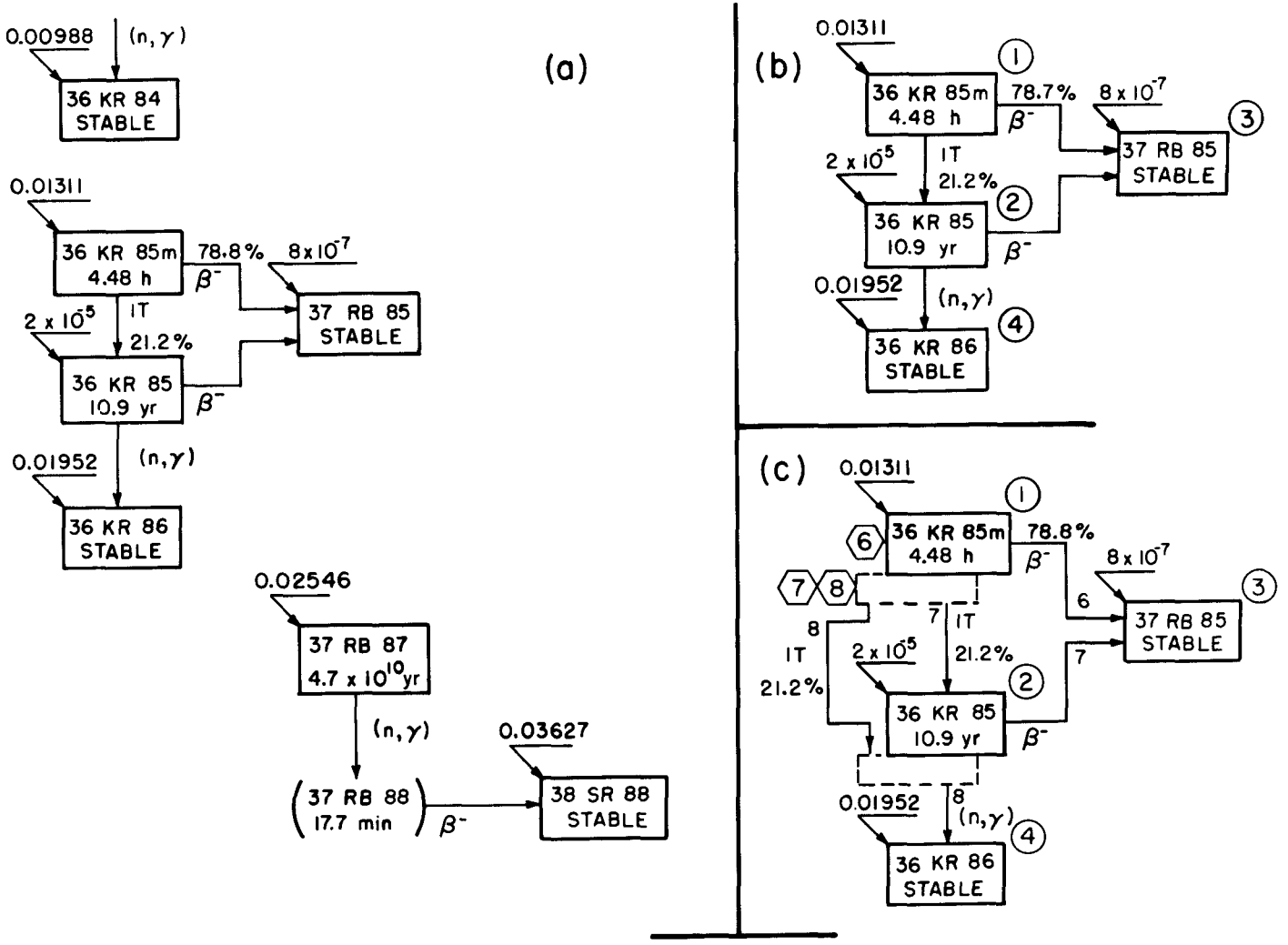

Fig. 2. Simplified fission product representation.

fraction and that of each of the lower Z isobars) plus the direct fission-yield fractions to $^{84m}_{37}Rb$ and $^{84}_{37}Rb$, which decay to $^{84}_{35}Kr$. Also, the direct fission yield fractions of the short-lived, low-Z isobars of mass 85 contribute only to $^{85m}_{36}Kr$ and not to $^{85}_{36}Kr$, due to the decay branching of $^{85}_{36}Br$. (The composition of effective fission-yield fractions for all nuclei included in the EPRI-CINDER data set are described in Sec. 3.)

Finally, it should be noted that $^{88}_{37}Rb$ appears in parentheses in Fig. 2(a). This representation is used solely to indicate the true path from nuclide to nuclide. It is actually assumed that $^{88}_{38}Sr$ is formed directly via neutron absorption by $^{87}_{37}Rb$; the chain structure does not treat the short-lived $^{88}_{37}Rb$ explicitly.

Mathematical Treatment

The nuclides shown in Fig. 1 were selected to illustrate the application of simplifications, reducing the problem to the scheme shown in Fig. 2(a). The 4 isolated nuclides of mass 85 and 86 will now serve to illustrate the mathematical treatment. These nuclides, shown in Fig. 2(b), have been numbered to facilitate notation.

In order to write the differential equations describing the concentrations N_i over a timestep Δt, we will start with the usual assumptions made in depletion codes. Fission-product microscopic cross sections for total neutron absorption $\sigma^j_{a_i}$ and radiative capture $\sigma^j_{c_i}$ are expressed as flux-weighted average values over each of J energy groups. For the fission products, $\sigma^j_{c_i}$ and $\sigma^j_{a_i}$ are essentially equal. However, the distinction is necessary for actinide chains and is retained in the following development. The few group fluxes, ϕ^j, are integrals of the energy-dependent neutron flux over each energy. These are assumed constant during a time increment Δt. The effects of the fission of each of K fissionable nuclides is accounted for by using constant, average fission rates S^k over Δt. Refering to Fig. 2(b), we may write the following expressions:

$$\frac{dN_1}{dt} = \sum_{k=1}^{K} y_1^k S^k - N_1 \left(\lambda_1 + \sum_{j=1}^{J} \sigma^j_{a_1} g_1^j \phi^j \right) \quad ,$$

$$\frac{dN_2}{dt} = \sum_{k=1}^{K} y_2^k S^k - N_2 \left(\lambda_2 + \sum_{j=1}^{J} \sigma_{a_2}^j g_2^j \phi^j \right) + N_1 \lambda_1 \alpha_{1,2} \quad ,$$

$$\frac{dN_3}{dt} = \sum_{k=1}^{K} y_3^k S^k - N_3 \sum_{j=1}^{j} \sigma_{a_3}^j g_3^j \phi^j + N_1 \lambda_1 \alpha_{1,3} + N_2 \lambda_2 \quad ,$$

$$\frac{dN_4}{dt} = \sum_{k=1}^{K} y_4^k S^k - N_4 \sum_{j=1}^{J} \sigma_{a_4}^j g_4^j \phi^j + N_2 \sum_{j=1}^{J} \sigma_{c_2}^j g_2^j \phi^j \quad , \qquad (1)$$

where

g_i^j = a spectrum or shielding factor of nuclide i in group j,

N_i = concentration of nuclide i,

y_i^k = effective fission yield fraction of nuclide i from fissionable nuclide k,

$\alpha_{i,i'}$ = branching fraction for the decay or absorption reaction of nuclide i producing nuclide i' (e.g., $\alpha_{1,2} = 0.212$),

λ_i = radioactive decay constant of nuclide i.

It is apparent that these differential equations, and thus their solutions, are not of the same form. Extending this observation to the situation of many coupled nuclides, one might anticipate the use of techniques involving matrix inversion and their associated difficulties with ill-conditioned matrices.

The linearization technique of CINDER permits an alternate solution to the problem. Here a number of linear chains are formed, each chain following one of the many combinations of neutron absorption and β^- decay sequences. The 3 linear paths required to describe the 4 mass 85 and 86 coupled nuclides are

shown in Fig. 2(c) as chains ⟨6⟩ , ⟨7⟩ , and ⟨8⟩ . The differential equations for each nuclide of each chain may be written, describing its temporal partial concentration due to a single decay or neutron absorption mode. Thus, each equation includes a single decay or reaction mode of gain but all modes of loss. The chains and associated equations are independent; partial concentrations in each chain may be calculated without regard to other chains. The total concentration of each nuclide is the sum of the partial concentrations from all chains in which that nuclide appears.

In some chains, the partial concentrations of certain nuclei are duplicated and, therefore, the partial concentrations must be summed with care. In the jargon of the code, these redundant partial concentrations must be "out-of-sum," although such concentrations are calculated since they contribute to the concentrations of subsequent nuclei in the chain. Out-of-sum partial concentrations are indicated by dashed symbols in Fig. 2(c) and subsequent figures.

A nuclides's effective fission-yield fraction must contribute to only one of its in-sum partial concentrations. Alternatively, the effective fission-yield fraction may be divided between a number of in-sum nuclide partial concentration expressions.

We may thus describe the partial concentrations of the nuclides of the three chains as follows:

Chain ⟨6⟩

$$\frac{dN_1}{dt} = \sum_{k=1}^{K} y_1^k S^k - N_1 \left(\lambda_1 + \sum_{j=1}^{J} \sigma_{a_1}^j g_1^j \phi^j \right) ,$$

$$\frac{dN_3}{dt} = - N_3 \left(\sum_{j=1}^{J} \sigma_{a_3}^j g_3^j \phi^j \right) + N_1 \lambda_1 \alpha_{1,3} , \qquad (2)$$

Chain ⟨7⟩

$$* \quad \frac{dN_1}{dt} = \sum_{k=1}^{K} y_1^k S^k - N_1 \left(\lambda_1 + \sum_{j=1}^{J} \sigma_{a_1}^j g_1^j \phi^j \right) ,$$

$$\frac{dN_2}{dt} = \sum_{k=1}^{K} y_2^k S^k - N_2 \left(\lambda_2 + \sum_{j=1}^{J} \sigma_{a_2}^j g_2^j \phi^j \right) + N_1 \lambda_1 \alpha_{1,2} ,$$

$$\frac{dN_3}{dt} = \sum_{k=1}^{K} y_3^k S^k - N_3 \left(\sum_{j=1}^{J} \sigma_{a_3}^j g_3^j \phi^j \right) + N_2 \lambda_2 , \qquad (3)$$

Chain ⟨8⟩

$$* \quad \frac{dN_1}{dt} = \sum_{k=1}^{K} y_1^k S^k - N_1 \left(\lambda_1 + \sum_{j=1}^{J} \sigma_{a_1}^j g_1^j \phi^j \right) ,$$

$$* \quad \frac{dN_2}{dt} = \sum_{k=1}^{K} y_2^k S^k - N_2 \left(\lambda_2 + \sum_{j=1}^{J} \sigma_{a_2}^j g_2^j \phi^j \right) + N_1 \lambda_1 \alpha_{1,2} ,$$

$$\frac{dN_4}{dt} = \sum_{k=1}^{K} y_4^k S^k - N_4 \left(\sum_{j=1}^{J} \sigma_{a_4}^j g_4^j \phi^j \right) + N_2 \sum_{j=1}^{J} \sigma_{c_2}^j g_2^j \phi^j , \qquad (4)$$

where the asterisk indicates that the corresponding nuclide partial concentration is out-of-sum. By adding the in-sum expressions for each nuclide, one may reconstruct the original set of differential equations [Eq. (1)]. This treatment by linear chains involves no loss in generality but results in a considerable increase in flexibility.

The partial concentration of now the i^{th} sequential nuclide in a linear chain is described by the following generalized sequence of coupled differential equations:

$$\frac{dN_i}{dt} = \sum_{k=1}^{K} y_i^k S^k - N_i(\lambda_i + A_i^a) + N_{i-1}\alpha_{i-1}\gamma_{i-1} \quad , \qquad (5)$$

$$i = 1,2,3,...$$

$A_i^a = \sum_{j=1}^{J} g_i^j \sigma_{a_i}^j \phi^j$, the neutron absorption rate per unit nuclide density.

$A_i^c = \sum_{j=1}^{J} g_i^j \sigma_{c_i}^j \phi^j$, the radiative capture rate per unit nuclide density, $A^c \equiv A^a - A^f$, where A^f is the fission rate analagous to A^a. (In lieu of branching fractions, fictitious fission cross sections may be specified for the fission products in order to achieve the correct activation cross sections leading to more than one daughter isomer.)

γ_{i-1} = either λ_{i-1}, A_{i-1}^a, or A_{i-1}^c, depending on coupling from precursor i-1.

α_{i-1} = fraction of specified coupling directly feeding nuclide i (e.g., in chain ⟨7⟩ , $\alpha_1 = 0.212$, $\alpha_2 = 1.0$).

This set of equations can equally well describe the fissionable nuclides and nuclides formed in the fuel chains (in which case, y = 0), as well as nuclides of the fission-product chains.

The general solution of the set (5) for the n^{th} nuclide, assuming a constant flux and an average constant fission rate during a time increment Δt, is shown in Ref. 3 to be:

$$N_n(t+\Delta t) = \sum_{m=1}^{n} \frac{1}{\alpha_n \gamma_n} \prod_{k=m}^{n} \gamma_k \alpha_k \left\{ \overline{y_m S} \left[\frac{1}{\prod_{\ell=m}^{n} (\lambda_\ell + A_\ell^a)} - \sum_{j=m}^{n} \frac{\exp[-(\lambda_j + A_j^a)\Delta t]}{(\lambda_j + A_j^a) \prod_{\substack{i=m \\ \neq j}}^{n} (\lambda_i + A_i^a - \lambda_j - A_j^a)} \right] + N_m(t) \left(\sum_{j=m}^{n} \frac{\exp[-(\lambda_j + A_j^a)\Delta t]}{\prod_{\substack{i=m \\ \neq j}}^{n} (\lambda_i + A_i^a - \lambda_j - A_j^a)} \right) \right\} \quad (6)$$

where $\overline{y_m S} = \overline{\sum_k y_m^k S^k}$ is the time-averaged yield rate to nuclide m during the interval Δt summed over all fissionable nuclides, k.

Section 3
FORMATION OF THE EPRI-CINDER DATA SET

The EPRI-CINDER Chain Structure

The selection of a chain structure follows the procedure described in Sec. 2. In preparing the EPRI-CINDER chain structure we have, of course, benefited by the existence of the chain structures of previously mentioned data sets.[3,4] A number of intermediate chain structures, with associated data, were generated, tested, and improved upon during the course of this work.

The resulting linear chain structure, shown in Fig. 3, uses 84 linear chains to describe 186 nuclides. A total of 484 partial nuclide concentrations, or

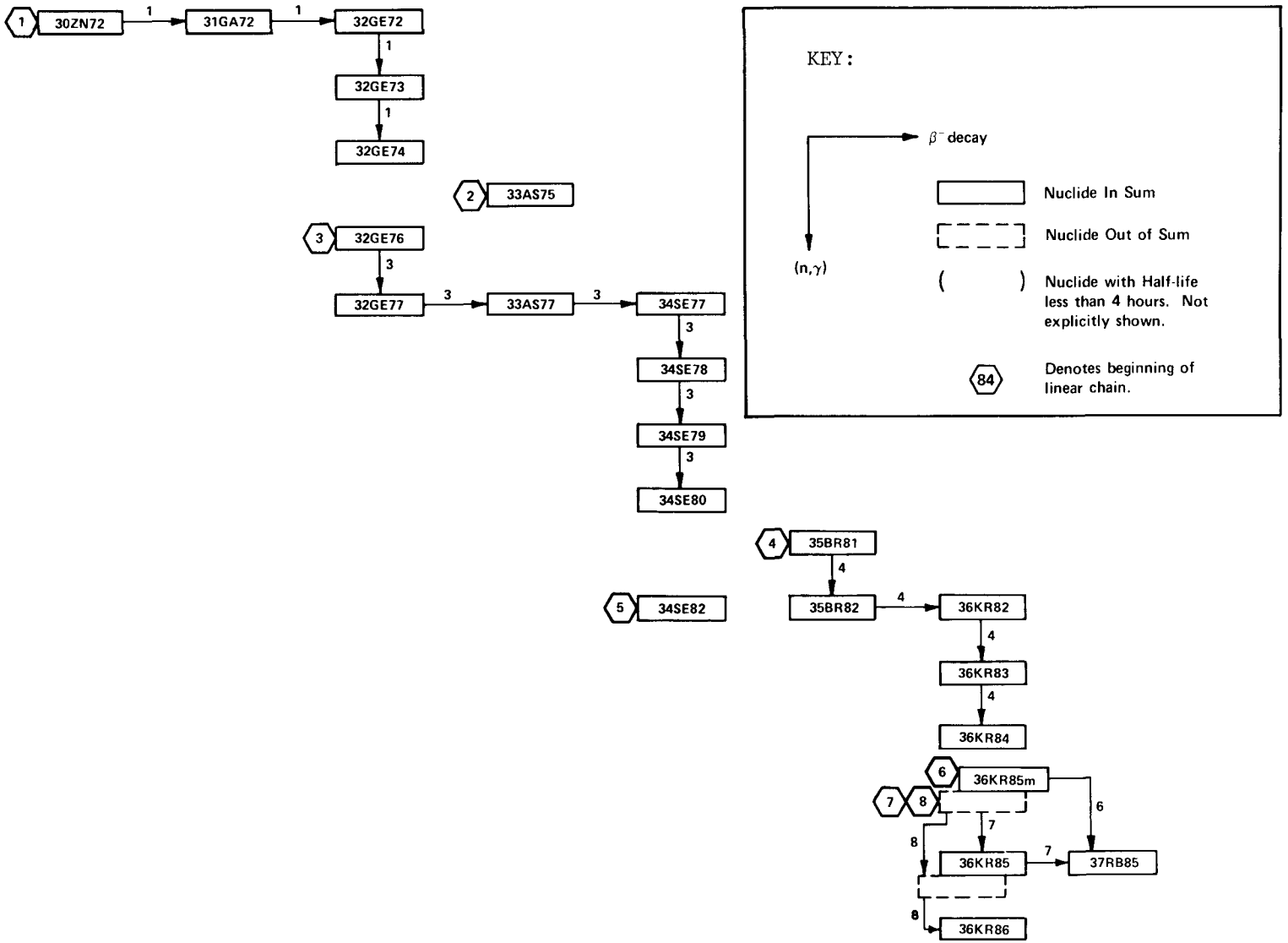

Fig. 3. EPRI-CINDER absorption-decay chain structure.

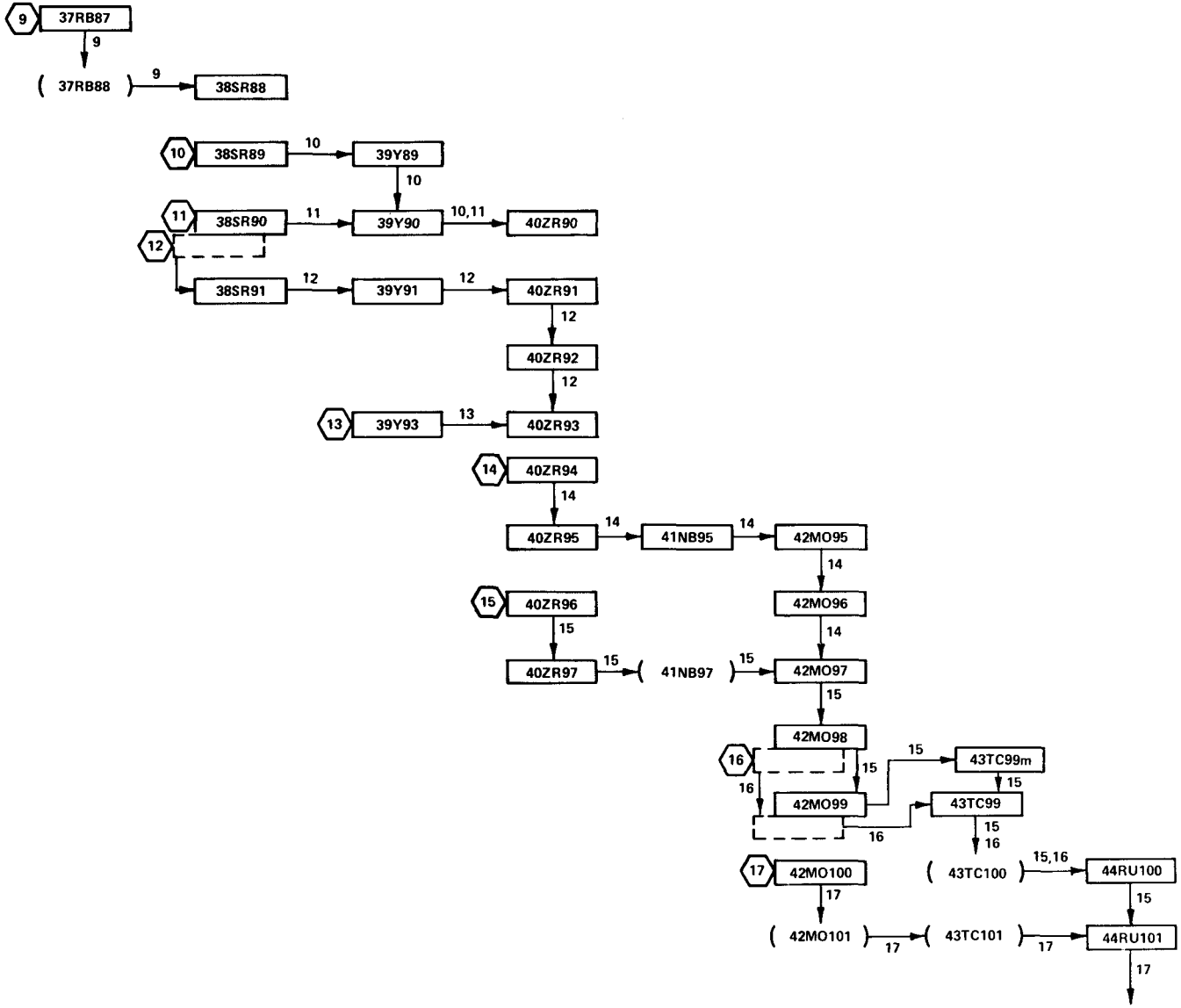

Fig. 3. (continued)

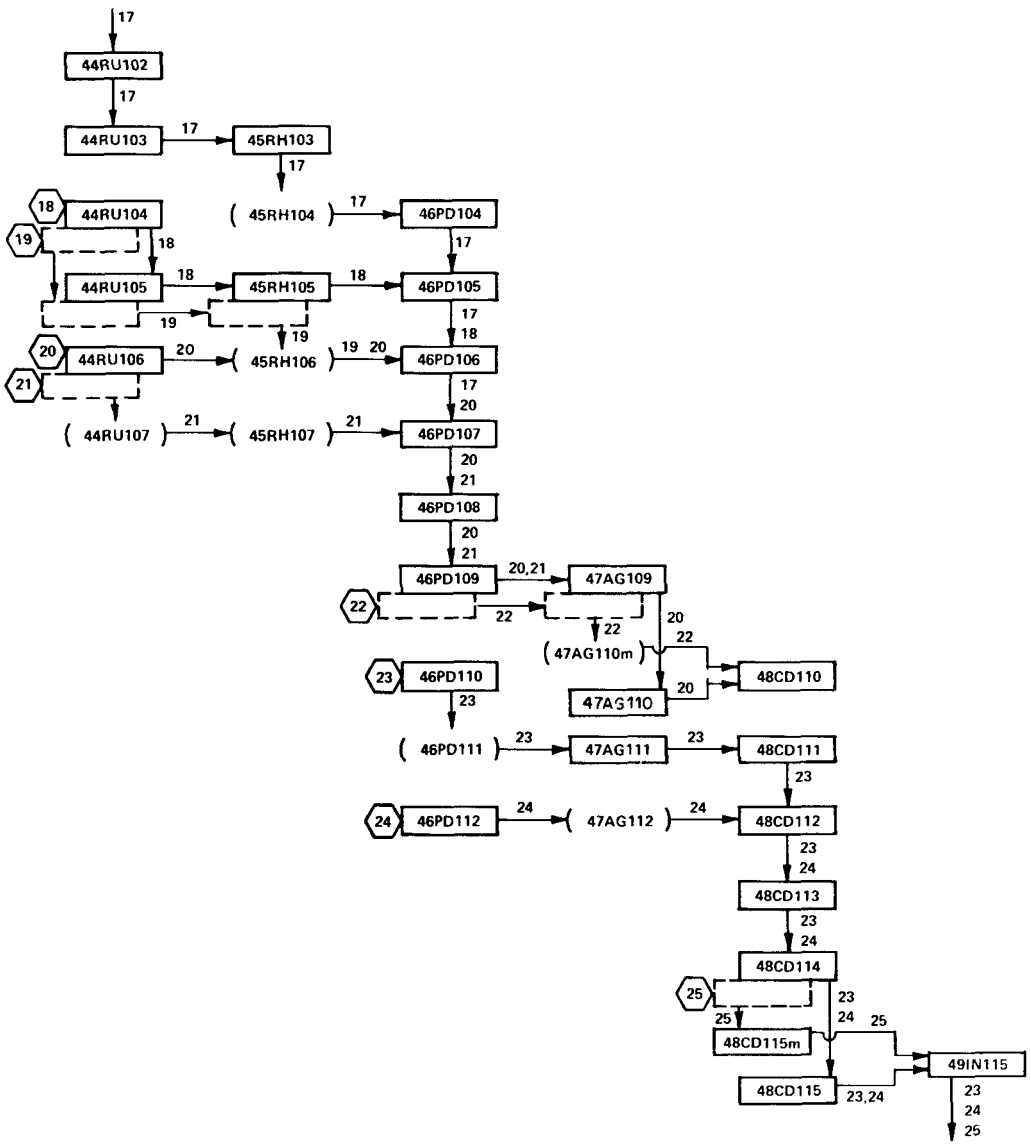

Fig. 3. (continued)

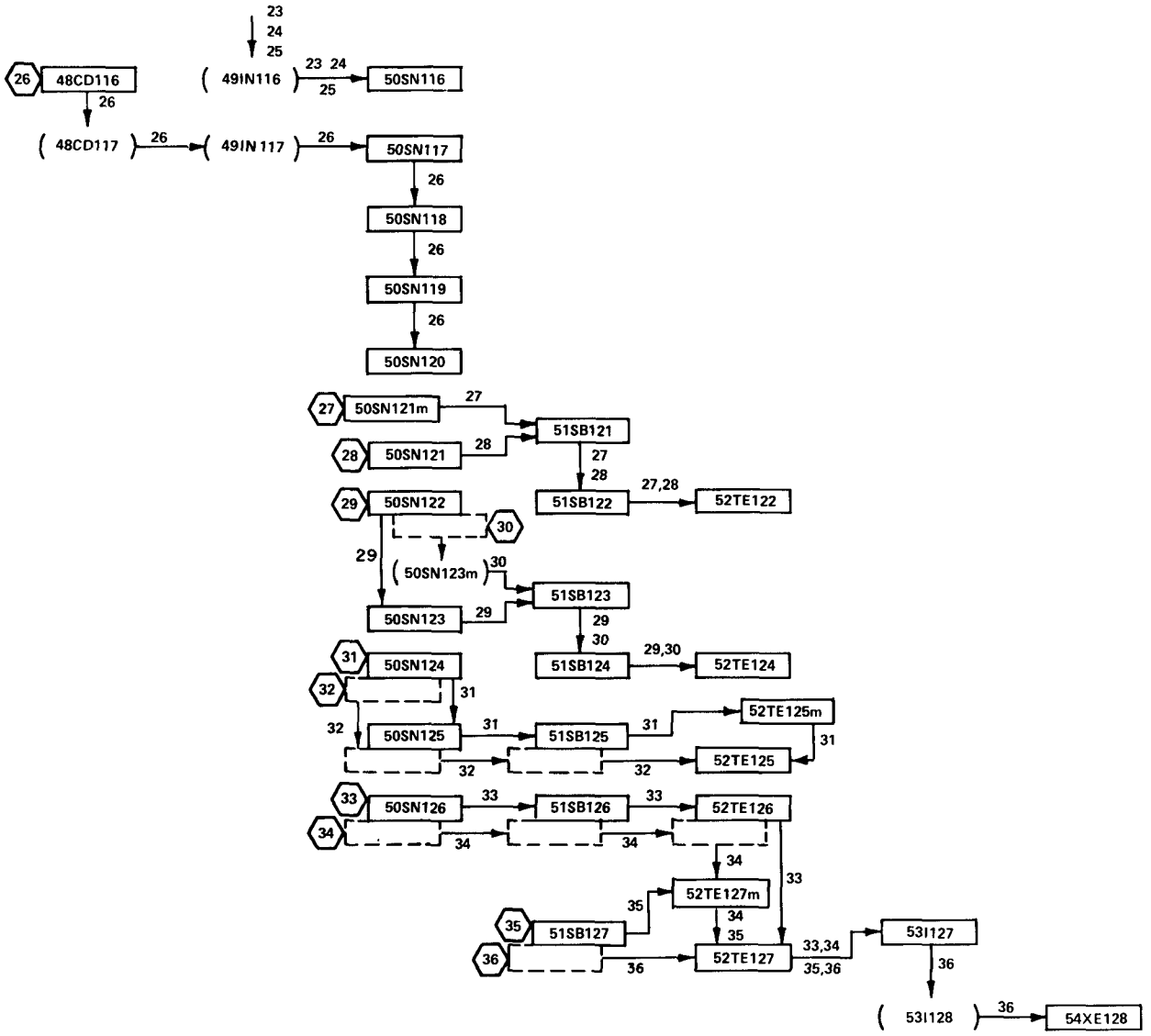

Fig. 3. (continued)

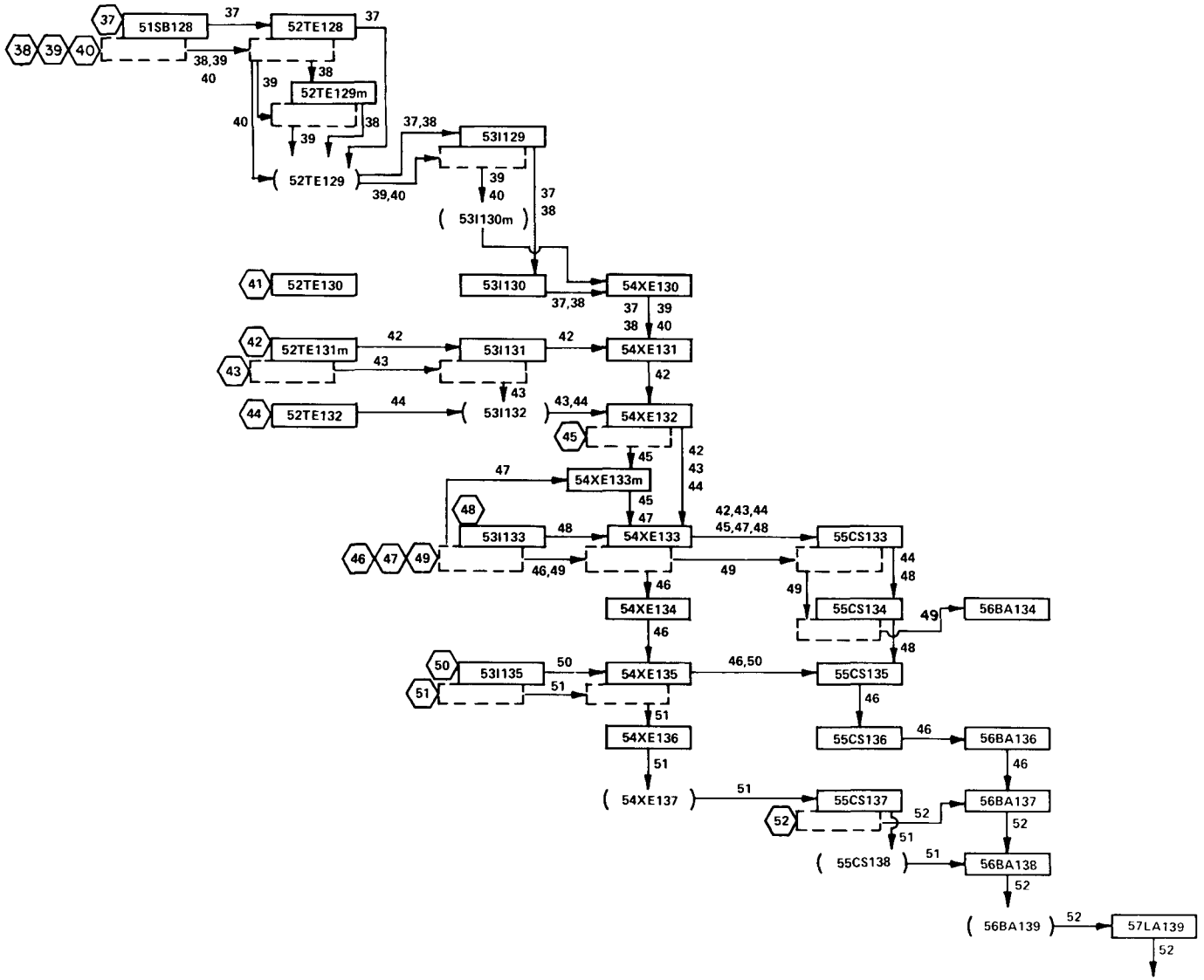

Fig. 3. (continued)

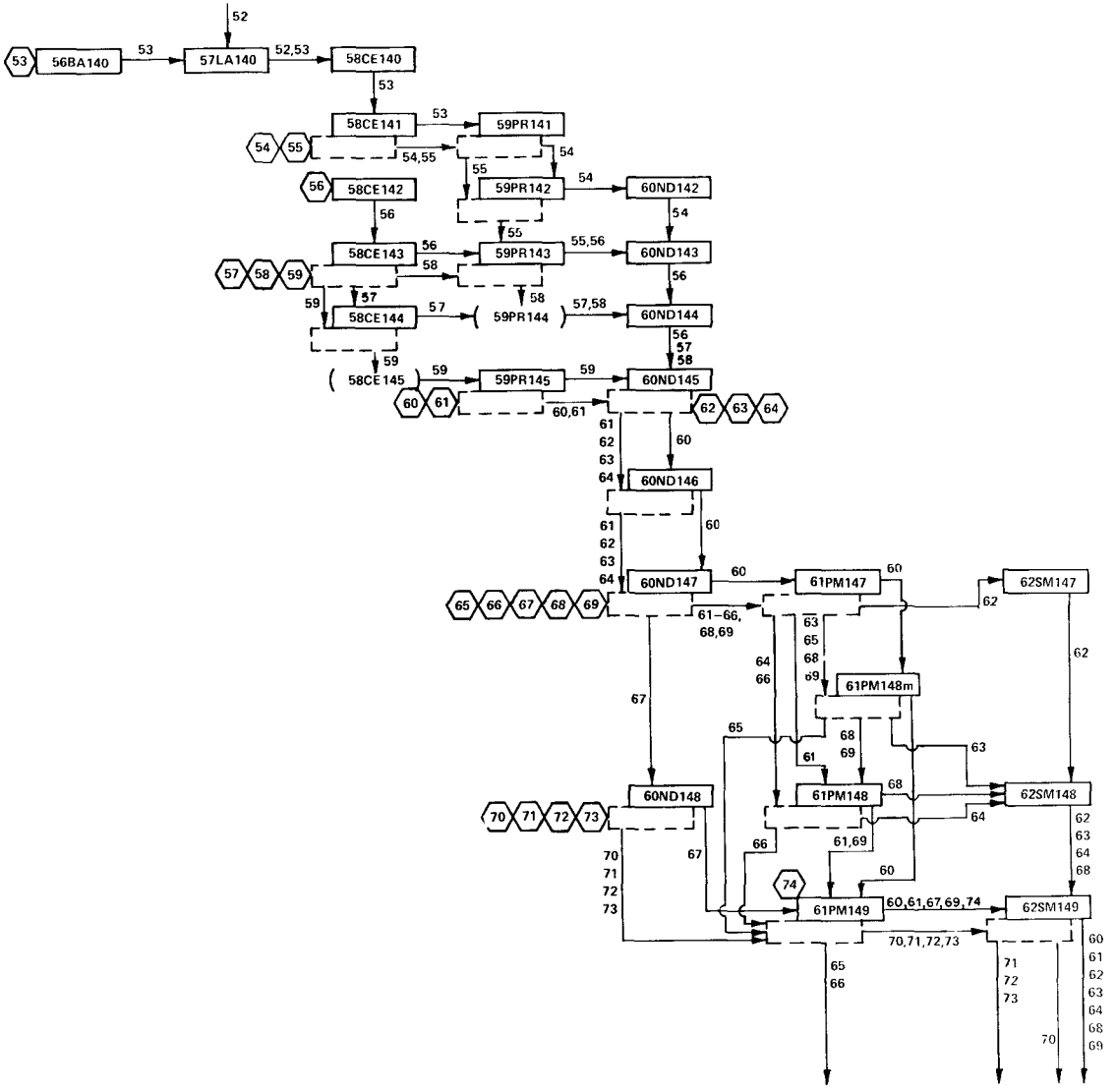

Fig. 3. (continued)

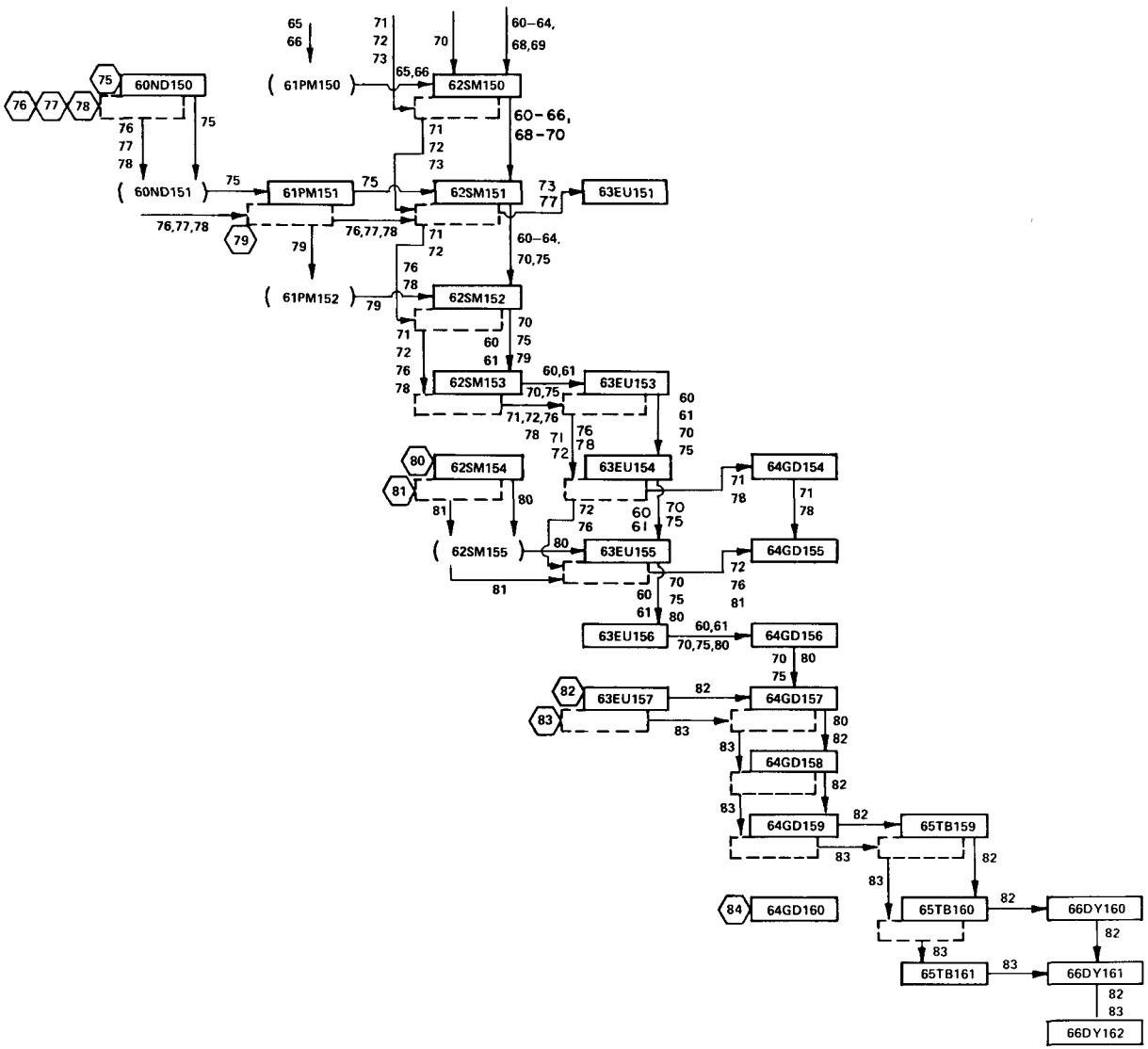

Fig. 3. (continued)

"linearized nuclides," are used. Examining this chain diagram, the chains ⟨6⟩, ⟨7⟩, ⟨8⟩ previously described are seen to be among the less complicated ones.

Users who wish to combine calculations using this EPRI-CINDER data set with those that already include the so-called "normal xenon" and "normal samarium"* may avoid duplicating these effects by placing all linearized nuclides of chains 50 and 74 out-of-sum.

Effective Fission Yield Fractions

In the formation of the chain structure for the EPRI-CINDER data set, we have assumed that all nuclides with half-lives less than four hours may be considered to decay instantaneously. The direct fission yield fractions associated with these nuclides are assigned to more stable isobars. The rationale supporting this assumption and that applied to the very high-Z isobars are described in Sec. 2.

We have also consistently ignored the delayed neutron (β^-n) mode of decay, which effectively transfers a portion of the effective yield fraction to a lower-mass nuclide. The inclusion of delayed-neutron branching in the composition of effective fission-yield fractions poses no problem, but this is effectively accounted for already in the yield data. The ENDF/B-IV fission-product data library included delayed-neutron branching fractions for 57 nuclei, each having a half-life less than 60 seconds. The ENDF/B-IV yield data file, describing the fractional independent fission yield to each of 824 nuclei, is based primarily on model calculations forced to agree with experimental data describing yields subsequent to delayed neutron emission. Therefore, the ENDF/B-IV fission yield fractions generally reflect the direct distribution of fission products following delayed-neutron emission. (NOTE: Future versions of ENDF/B will use independent yields prior to delayed neutron emission. However, examination of the fission products decaying by delayed-neutron (β^-n) emission shows that for $^{235}_{92}$U thermal fission the effective yield to any mass would be changed only slightly by the alternate assumption that ENDF/B fission-yield fractions reflect the direct distribution of

*"Normal xenon" and "normal samarium" refer to $^{135}_{34}$Xe and $^{149}_{62}$Sm formed, respectively, by the mass 135 and 149 fission yield.

fission products prior to (β^-n) emission. Yield computations would then explicitly include delayed neutron branching. For ENDF/B-IV, effective yields to only 9 mass chains would be decreased by greater than 1%. The greatest effect would be a 3.4% decrease in the effective yield to $^{89}_{38}Sr$ due to delayed neutron branching from $^{89}_{34}Se$ and $^{89}_{35}Br$.)

The descriptions of the formation of effective fission-yield fractions to each of the 186 nuclides of the EPRI-CINDER chain structures are given in Table 1. These descriptions are used to calculate effective fission-yield fractions for each of 10 combinations of fissionable nuclides and neutron fission energies.

Section 4
NUCLEAR DATA

The ENDF/B-IV Fission-Product Data

Fission-product data are given for some 824 nuclides in the ENDF/B-IV fission-product library. Of these, 181 nuclides (MATs) are complete with evaluated neutron cross sections expressed as a function of neutron energy over the range 1 X 10^{-5} eV-20 MeV, using tabulated values, resonance parameters, and various interpolation schemes. Each of these 181 nuclides have evaluated neutron cross sections for total (MT=1), elastic (MT=2), total inelastic (MT=4), and radiative capture (MT=102) reactions. Thirty-six of these have additional evaluated cross sections for other neutron-absorption reactions, such as (n,p), (n,α), etc. The ENDF/B fission-product data files also include decay and decay-branching data. These parameters, including a few corrections, have been concisely listed in Ref. 5, which also includes branching by neutron absorption.

Direct fission yield fractions are tabulated in the ENDF/B-IV fission-product library for the following combinations of fissionable nuclides and incident neutron spectra:

Nuclide	Spectrum
$^{232}_{90}Th$	Fast
$^{233}_{92}U$	Thermal
$^{235}_{92}U$	Thermal
$^{235}_{92}U$	Fast
$^{235}_{92}U$	14 MeV
$^{238}_{92}U$	Fast
$^{238}_{92}U$	14 MeV
$^{239}_{94}Pu$	Thermal
$^{239}_{94}Pu$	Fast
$^{241}_{94}Pu$	Thermal

From these files we must extract or process the following:

- Four-group neutron absorption cross sections for each of the fission-product nuclei.
- Effective fission-yield fractions to each of the fission-product nuclei for each of the 10 combinations of fissionable nuclei and neutron-fission energies.
- Radioactive decay constants for all fission-product nuclei.
- Branching fractions for all decay and absorption couplings.

TABLE 1

DESCRIPTION OF YIELDS 84-CHAIN STRUCTURE

NOTATION----

DY(Z,A,S)=DIRECT YIELD TO NUCLIDE WITH MASS A, CHARGE Z AND STATE S, WHERE 0=GROUND STATE AND 1=METASTABLE STATE

DH(Z,A,S)=DIRECT YIELD TO NUCLIDE WITH MASS A, CHARGE Z AND STATE S, PLUS THE DIRECT YIELD TO EACH NUCLIDE OF THIS MASS WITH HIGHER Z. THE HIGHER-Z ISOBARS ARE TREATED AS IF TO DECAY (B+ OR EC) INSTANTANEOUSLY

CY(Z,A) =CUMULATIVE YIELD, SUM OF DIRECT YIELDS TO NUCLEI OF MASS A AND CHARGE Z OR LESS. LOW-Z ISOBARS ARE TREATED AS IF TO DECAY (B-,IT) INSTANTANEOUSLY.

TY(A) =TOTAL MASS YIELD, THE SUM OF DIRECT YIELDS TO ALL NUCLEI OF MASS A

FRACTIONAL YIELD QUANTITIES SHOWN BELOW RESULT FROM DECAY BRANCHING TO AND FROM GROUND AND METASTABLE STATES OF SHORT LIVED PRECURSORS NOT EXPLICITLY INCLUDED IN THE CHAIN STRUCTURE. DELAYED NEUTRON BRANCHING IS IGNORED, FOLLOWING THE DISCUSSION OF SECTION 3.

NUCLIDE	Z	A	S	YIELD DESCRIPTION
ZN 72	30	72	0	1.000*CY(30, 72)
GA 72	31	72	0	1.000*DY(31, 72,0) +1.000*DY(31, 72,1)
GE 72	32	72	0	1.000*DH(32, 72,0)
GE 73	32	73	0	1.000*CY(32, 73)
GE 74	32	74	0	1.000*CY(32, 74)
GE 76	32	76	0	1.000*CY(32, 76)
GE 77	32	77	0	.305*CY(31, 77) + .210*DY(32, 77,1) +1.000*DY(32, 77,0)
AS 75	33	75	0	1.000*CY(33, 75)
AS 77	33	77	0	.695*CY(31, 77) + .790*DY(32, 77,1) +1.000*DY(33, 77,0)
SE 77	34	77	0	1.000*DY(34, 77,0) +1.000*DH(34, 77,1)
SE 78	34	78	0	1.000*CY(34, 78) +1.000*DY(35, 78,0)
SE 79	34	79	0	1.000*CY(34, 79)
SE 80	34	80	0	1.000*CY(34, 80)

NUCLIDE	Z	A	S	YIELD DESCRIPTION
SE 82	34	82	0	1.000*CY(34, 82)
BR 81	35	81	0	1.000*CY(35, 81)
BR 82	35	82	0	1.000*DY(35, 82,0) +1.000*DY(35, 82,1)
KR 82	36	82	0	1.000*DH(36, 82,0)
KR 83	36	83	0	1.000*TY(83)
KR 84	36	84	0	1.000*CY(36, 84) +1.000*DY(37, 84,0) +1.000*DY(37, 84,1)
KR 85M	36	85	1	1.000*CY(35, 85) +1.000*DY(36, 85,1)
KR 85	36	85	0	1.000*DY(36, 85,0)
KR 86	36	86	0	1.000*CY(36, 86)
RB 85	37	85	0	1.000*DH(37, 85,0)
RB 87	37	87	0	1.000*CY(37, 87)
SR 88	38	88	0	1.000*CY(38, 88)
SR 89	38	89	0	1.000*CY(38, 89)
SR 90	38	90	0	1.000*CY(38, 90)
SR 91	38	91	0	1.000*CY(38, 91)
Y 89	39	89	0	1.000*DY(39, 89,0) +1.000*DH(39, 89,1)
Y 90	39	90	0	1.000*DY(39, 90,0) +1.000*DY(39, 90,1)
Y 91	39	91	0	1.000*DY(39, 91,0) +1.000*DY(39, 91,1)
Y 93	39	93	0	1.000*CY(39, 93)
ZR 90	40	90	0	1.000*DY(40, 90,0) +1.000*DH(40, 90,1)
ZR 91	40	91	0	1.000*DY(40, 91,0)
ZR 92	40	92	0	1.000*CY(40, 92)
ZR 93	40	93	0	1.000*DY(40, 93,0)
ZR 94	40	94	0	1.000*CY(40, 94)
ZR 95	40	95	0	1.000*CY(40, 95)
ZR 96	40	96	0	1.000*CY(40, 96)
ZR 97	40	97	0	1.000*CY(40, 97)
NB 95	41	95	0	1.000*DY(41, 95,0) +1.000*DY(41, 95,1)
MO 95	42	95	0	1.000*DH(42, 95,0)
MO 96	42	96	0	1.000*DY(42, 96,0) +1.000*DY(41, 96,0) +1.000*DY(43, 96,0) +1.000*DY(43, 96,1)
MO 97	42	97	0	1.000*DY(42, 97,0) +1.000*DY(41, 97,0) +1.000*DY(41, 97,1)
MO 98	42	98	0	1.000*CY(42, 98)
MO 99	42	99	0	1.000*CY(42, 99)
MO100	42	100	0	1.000*CY(42,100)
TC 99M	43	99	1	1.000*DY(43, 99,1)

NUCLIDE	Z	A	S	YIELD DESCRIPTION
TC 99	43	99	0	1.000*DY(43, 99,0)
RU100	44	100	0	1.000*DH(43,100,0)
RU101	44	101	0	1.000*CY(44,101)
RU102	44	102	0	1.000*CY(44,102)
RU103	44	103	0	1.000*CY(44,103)
RU104	44	104	0	1.000*CY(44,104)
RU105	44	105	0	1.000*CY(44,105)
RU106	44	106	0	1.000*CY(44,106)
RH103	45	103	0	1.000*DY(45,103,0) +1.000*DH(45,103,1)
RH105	45	105	0	1.000*DY(45,105,0) +1.000*DY(45,105,1)
PD104	46	104	0	1.000*DY(45,104,0 +1.000*DH(45,104,1)
PD105	46	105	0	1.000*DH(46,105,0)
PD106	46	106	0	1.000*DY(45,106,0) +1.000*DY(45,106,1) +1.000*DY(46,106,0) +1.000*DY(47,106,0) +1.000*DY(47,106,1)
PD107	46	107	0	1.000*CY(46,107)
PD108	46	108	0	1.000*CY(46,108)
PD109	46	109	0	1.000*CY(46,109)
PD110	46	110	0	1.000*CY(46,110)
PD112	46	112	0	1.000*CY(46,112)
AG109	47	109	0	1.000*DY(47,109,0) +1.000*DH(47,109,1)
AG110	47	110	0	1.000*DY(47,110,0)
AG111	47	111	0	1.000*CY(47,111)
CD110	48	110	0	1.000*DH(47,110,1)
CD111	48	111	0	1.000*DY(48,111,0) +1.000*DH(48,111,1)
CD112	48	112	0	1.000*DY(47,112,0) +1.000*DY(48,112,0)
CD113	48	113	0	1.000*CY(48,113)
CD114	48	114	0	1.000*CY(48,114)
CD115M	48	115	1	.135*CY(46,115) + .085*DY(47,115,0) + .270*DY(47,115,1) +1.000*DY(48,115,1)
CD115	48	115	0	.865*CY(46,115) + .915*DY(47,115,0) + .730*DY(47,115,1) +1.000*DY(48,115,0)
CD116	48	116	0	1.000*CY(48,116)
IN115	49	115	0	1.000*DY(49,115,0) +1.000*DY(49,115,1)
SN116	50	116	0	1.000*DY(49,116,0) +1.000*DH(49,116,1)
SN117	50	117	0	1.000*TY(117)
SN118	50	118	0	1.000*TY(118)
SN119	50	119	0	1.000*TY(119)

NUCLIDE	Z	A	S	YIELD DESCRIPTION		
SN120	50	120	0	1.000*CY(51,120)		
SN121M	50	121	1	1.000*DY(50,121,1)		
SN121	50	121	0	1.000*CY(49,121)	+1.000*DY(50,121,0)	
SN122	50	122	0	1.000*CY(50,122)		
SN123	50	123	0	.500*CY(49,123)	+1.000*DY(50,123,0)	
SN124	50	124	0	1.000*CY(50,124)		
SN125	50	125	0	1.000*CY(50,125)		
SN126	50	126	0	1.000*CY(50,126)		
SB121	51	121	0	1.000*DH(51,121,0)		
SB122	51	122	0	1.000*DY(51,122,0)	+1.000*DY(51,122,1)	
SB123	51	123	0	.500*CY(49,123)	+1.000*DY(50,123,1)	+1.000*DY(51,123,0)
SB124	51	124	0	1.000*DY(51,124,0)	+1.000*DY(51,124,1)	
SB125	51	125	0	1.000*DY(51,125,0)		
SB126	51	126	0	1.000*DY(51,126,0)	+ .140*DY(51,126,1)	
SB127	51	127	0	1.000*CY(51,127)		
SB128	51	128	0	1.000*DY(51,128,0)		
TE122	52	122	0	1.000*DH(52,122,0)		
TE124	52	124	0	1.000*DY(52,124,0)	+1.000*DY(53,124,0)	
TE125	52	125	0	1.000*DH(52,125,0)		
TE125M	52	125	1	1.000*DY(52,125,1)		
TE126	52	126	0	.860*DY(51,126,1)	+1.000*DY(52,126,0)	+1.000*DY(53,126,0)
TE127	52	127	0	1.000*DY(52,127,0)		
TE127M	52	127	1	1.000*DY(52,127,1)		
TE128	52	128	0	1.000*CY(50,128)	+1.000*DY(51,128,1)	+1.000*DY(52,128,0)
TE129M	52	129	1	.240*CY(51,129)	+1.000*DY(52,129,1)	
TE130	52	130	0	1.000*CY(52,130)		
TE131M	52	131	1	.068*CY(51,131)	+1.000*DY(52,131,1)	
TE132	52	132	0	1.000*CY(52,132)		
I127	53	127	0	1.000*DH(53,127,0)		
I129	53	129	0	.760*CY(51,129)	+1.000*DY(52,129,0)	+1.000*DY(53,129,0)
I130	53	130	0	1.000*DY(53,130,0)		
I131	53	131	0	.932*CY(51,131)	+1.000*DY(52,131,0)	+1.000*DY(53,131,0)
I133	53	133	0	1.000*CY(53,133)		
I135	53	135	0	1.000*CY(53,135)		
XE128	54	128	0	1.000*DH(53,128,0)		

NUCLIDE	Z	A	S	YIELD DESCRIPTION
XE130	54	130	0	1.000*DY(54,130,0)
XE131	54	131	0	1.000*DY(54,131,0) +1.000*DH(54,131,1)
XE132	54	132	0	1.000*DY(53,132,0) +1.000*DY(54,132,0) +1.000*DY(54,132,1) +1.000*DY(55,132,0)
XE133	54	133	0	1.000*DY(54,133,0)
XE133M	54	133	1	1.000*DY(54,133,1)
XE134	54	134	0	1.000*CY(54,134)
XE135	54	135	0	1.000*DY(54,135,0) +1.000*DY(54,135,1)
XE136	54	136	0	1.000*CY(54,136)
CS133	55	133	0	1.000*DH(55,133,0)
CS134	55	134	0	1.000*DY(55,134,0) +1.000*DY(55,134,1)
CS135	55	135	0	1.000*DY(55,135,0) +1.000*DY(55,135,1)
CS136	55	136	0	1.000*DY(55,136,0)
CS137	55	137	0	1.000*CY(55,137)
BA134	56	134	0	1.000*DH(56,134,0)
BA136	56	136	0	1.000*DY(56,136,0) +1.000*DY(56,136,1) +1.000*DY(57,136,0) +1.000*DY(57,136,1)
BA137	56	137	0	1.000*DY(56,137,0) +1.000*DH(56,137,1)
BA138	56	138	0	1.000*TY(138)
BA140	56	140	0	1.000*CY(56,140)
LA139	57	139	0	1.000*CY(57,139)
LA140	57	140	0	1.000*DY(57,140,0)
CE140	58	140	0	1.000*DH(58,140,0)
CE141	58	141	0	1.000*CY(58,141)
CE142	58	142	0	1.000*CY(58,142)
CE143	58	143	0	1.000*CY(58,143)
CE144	58	144	0	1.000*CY(58,144)
PR141	59	141	0	1.000*DH(59,141,0)
PR142	59	142	0	1.000*DY(59,142,0) +1.000*DY(59,142,1)
PR143	59	143	0	1.000*DY(59,143,0)
PR145	59	145	0	1.000*CY(59,145)
ND142	60	142	0	1.000*DH(60,142,0)
ND143	60	143	0	1.000*DH(60,143,0)
ND144	60	144	0	1.000*DY(59,144,0) +1.000*DY(59,144,1) +1.000*DY(60,144,0) +1.000*DY(61,144,0)
ND145	60	145	0	1.000*DH(60,145,0)
ND146	60	146	0	1.000*CY(60,146)
ND147	60	147	0	1.000*CY(60,147)

NUCLIDE	Z	A	S	YIELD DESCRIPTION
ND148	60	148	0	1.000*CY(60,148)
ND150	60	150	0	1.000*CY(60,150)
PM147	61	147	0	1.000*DY(61,147,0)
PM148	61	148	0	1.000*DY(61,148,0)
PM148M	61	148	1	1.000*DY(61,148,1)
PM149	61	149	0	1.000*CY(61,149)
PM151	61	151	0	1.000*CY(61,151)
SM147	62	147	0	1.000*DH(62,147,0)
SM148	62	148	0	1.000*DH(62,148,0)
SM149	62	149	0	1.000*DH(62,149,0)
SM150	62	150	0	1.000*DY(61,150,0) +1.000*DY(62,150,0)
SM151	62	151	0	1.000*DY(62,151,0)
SM152	62	152	0	1.000*CY(62,152)
SM153	62	153	0	1.000*CY(62,153)
SM154	62	154	0	1.000*CY(62,154)
EU151	63	151	0	1.000*DY(63,151,0) +1.000*DH(63,151,1)
EU153	63	153	0	1.000*DH(63,153,0)
EU154	63	154	0	1.000*DY(63,154,0)
EU155	63	155	0	1.000*CY(63,155)
EU156	63	156	0	1.000*CY(63,156)
EU157	63	157	0	1.000*CY(63,157)
GD154	64	154	0	1.000*DY(64,154,0) +1.000*DY(65,154,0) +1.000*DY(65,154,1)
GD155	64	155	0	1.000*DH(64,155,0)
GD156	64	156	0	1.000*DY(64,156,0) +1.000*DY(65,156,0) +1.000*DY(65,156,1)
GD157	64	157	0	1.000*DY(64,157,0)
GD158	64	158	0	1.000*CY(64,158)
GD159	64	159	0	1.000*CY(64,159)
GD160	64	160	0	1.000*CY(64,160)
TB159	65	159	0	1.000*DY(65,159,0)
TB160	65	160	0	1.000*DY(65,160,0)
TB161	65	161	0	1.000*CY(65,161)
DY160	66	160	0	1.000*DH(66,160,0)
DY161	66	161	0	1.000*DH(66,161,0)
DY162	66	162	0	1.000*CY(66,162) +1.000*DY(67,162,0) +1.000*DY(67,162,1)

Chain Nuclide Data

The EPRI-CINDER code accepts four-group flux-weighted average cross sections. The EPRI four-group cross-section energy structure is defined as follows:

$1.000000000 \times 10^{7}$ eV

Group 1

$8.208499862 \times 10^{5}$ eV

Group 2

$5.530843701 \times 10^{3}$ eV

Group 3

$6.250600000 \times 10^{-1}$ eV

Group 4

$1.000000000 \times 10^{-5}$ eV

Cross sections may be processed directly into the EPRI four-group structure or into a group structure containing many fine groups, from which the four-group cross sections may be collapsed. Few-group cross sections collapsed from a fine-group cross section set, using the same flux-weighting function in cross-section processing and collapsing, are identical to values processed directly into the few-group structure with energy bounds common to the fine-group structure.

We have chosen to process all cross sections in the Power Reactor Studies (PRS) 154-Group Structure,[6] listed in Table 2. The flux-weighting function used in cross-section processing and subsequent collapsing is the PRS Flux Weighting Function,[7] shown in Fig. 4. The PRS Flux Weighting Function, typical of light water reactors, is described by 115 pairs of flux- and neutron-energy values listed in Table 3, between which log-log interpolation is used.

All cross sections listed in the ENDF/B fission-product library were processed into the PRS 154-Group Structure, using the PRS Flux Weighting Function by the NJOY cross-section processing system.[8] Thirty-six nuclides (MATs) appearing on both the ENDF/B-IV fission-product and general-purpose data files were processed from the latter at temperatures of 0 and 900 K, using PENDF[9] files retained from previous processing. The remaining 145 MATs were processed from the fission-product data files at 0 and 1000 K.

All cross section reaction (MT) tabulations were thus processed into the fine-group structure at, effectively, two temperatures. These cross sections were

TABLE 2

THE 154-GROUP PRS NEUTRON MULTIGROUP STRUCTURE

GROUP NO.	UPPER ENERGY BOUND,(EV)	GROUP ENERGY WIDTH,(EV)	LETHARGY	LETHARGY DIFFERENCE	CORRESPONDS WITH UPPER BOUND OF GROUPS IN THE FOLLOWING GAMI 68	GRANIT 48	LASER 35	LASL 30	EPRI 4
1	2.000000000E+07	1.7788120E+06	-6.931472E-01	9.314718E-02					
2	1.822118800E+07	1.3165995E+06	-6.000000E-01	7.500000E-02					
3	1.690458848E+07	1.9863415E+06	-5.250000E-01	1.250000E-01				1	
4	1.491824698E+07	1.4196589E+06	-4.000000E-01	1.000000E-01				2	
5	1.349858808E+07	1.5861259E+06	-3.000000E-01	1.250000E-01				3	
6	1.191246217E+07	1.9124622E+06	-1.750000E-01	1.750000E-01				4	
7	1.000000000E+07	2.2119922E+06	0.	2.500000E-01	1			5	1
8	7.788007831E+06	1.7227012E+06	2.500000E-01	2.500000E-01	2			6	
9	6.065306597E+06	1.3416411E+06	5.000000E-01	2.500000E-01	3			7	
10	4.723665527E+06	1.0448711E+06	7.500000E-01	2.500000E-01	4				
11	3.678794412E+06	8.1374644E+05	1.000000E+00	2.500000E-01	5			8	
12	2.865047969E+06	6.3374637E+05	1.250000E+00	2.500000E-01	6			9	
13	2.231301601E+06	4.9356217E+05	1.500000E+00	2.500000E-01	7			10	
14	1.737739435E+06	3.8438660E+05	1.750000E+00	2.500000E-01	8			11	
15	1.353352832E+06	2.9936059E+05	2.000000E+00	2.500000E-01	9			12	
16	1.053992246E+06	1.0030062E+05	2.250000E+00	1.000000E-01	10				
17	9.536916222E+05	1.3284164E+05	2.350000E+00	1.500000E-01					
18	8.208499862E+05	7.8114204E+04	2.500000E+00	1.000000E-01	11			13	2
19	7.427357821E+05	1.0345717E+05	2.600000E+00	1.500000E-01					
20	6.392786121E+05	6.0835403E+04	2.750000E+00	1.000000E-01	12				
21	5.784432087E+05	8.0572525E+04	2.850000E+00	1.500000E-01					
22	4.978706837E+05	4.7378660E+04	3.000000E+00	1.000000E-01	13			14	
23	4.504920239E+05	6.2749946E+04	3.100000E+00	1.500000E-01					
24	3.877420783E+05	3.6898537E+04	3.250000E+00	1.000000E-01	14				
25	3.508435410E+05	4.8869707E+04	3.350000E+00	1.500000E-01					
26	3.019738342E+05	2.8736610E+04	3.500000E+00	1.000000E-01	15			15	
27	2.732372245E+05	3.8059766E+04	3.600000E+00	1.500000E-01					
28	2.351774586E+05	2.2380094E+04	3.750000E+00	1.000000E-01	16				
29	2.127973644E+05	2.9640976E+04	3.850000E+00	1.500000E-01					
30	1.831563889E+05	4.0514050E+04	4.000000E+00	2.500000E-01	17			16	
31	1.426423391E+05	3.1552374E+04	4.250000E+00	2.500000E-01	18				
32	1.110899654E+05	2.4573013E+04	4.500000E+00	2.500000E-01	19				
33	8.651695203E+04	1.9137482E+04	4.750000E+00	2.500000E-01	20				
34	6.737946999E+04	1.4904286E+04	5.000000E+00	2.500000E-01	21			17	
35	5.247518399E+04	1.1607470E+04	5.250000E+00	2.500000E-01	22				
36	4.086771438E+04	9.0399064E+03	5.500000E+00	2.500000E-01	23				
37	3.182780797E+04	3.7398660E+03	5.750000E+00	1.250000E-01	24				
38	2.808794195E+04	2.0295368E+03	5.875000E+00	7.500000E-02					

GROUP NO.	UPPER ENERGY BOUND,(EV)	GROUP ENERGY WIDTH,(EV)	LETHARGY	LETHARGY DIFFERENCE	CORRESPONDS WITH UPPER BOUND OF GROUPS IN THE FOLLOWING GAMI 68	GRANIT 48	LASER 35	LASL 30	EPRI 4
39	2.605840518E+04	1.2708834E+03	5.950000E+00	5.000000E-02					
40	2.478752177E+04	1.2089017E+03	6.000000E+00	5.000000E-02	25			18	
41	2.357862006E+04	4.2740787E+03	6.050000E+00	2.000000E-01					
42	1.930454136E+04	4.2701494E+03	6.250000E+00	2.500000E-01	26				
43	1.503439193E+04	3.3255957E+03	6.500000E+00	2.500000E-01	27				
44	1.170879621E+04	2.5899766E+03	6.750000E+00	2.500000E-01	28				
45	9.118819656E+03	2.0170758E+03	7.000000E+00	2.500000E-01	29			19	
46	7.101743888E+03	1.5709002E+03	7.250000E+00	2.500000E-01	30				
47	5.530843701E+03	1.2234183E+03	7.500000E+00	2.500000E-01	31				3
48	4.307425406E+03	9.5279913E+02	7.750000E+00	2.500000E-01	32				
49	3.354626279E+03	7.4204071E+02	8.000000E+00	2.500000E-01	33			20	
50	2.612585573E+03	5.7790188E+02	8.250000E+00	2.500000E-01	34				
51	2.034683690E+03	4.5007044E+02	8.500000E+00	2.500000E-01	35				
52	1.584613251E+03	3.5051521E+02	8.750000E+00	2.500000E-01	36				
53	1.234098041E+03	2.7298152E+02	9.000000E+00	2.500000E-01	37			21	
54	9.611165206E+02	2.1259822E+02	9.250000E+00	2.500000E-01	38				
55	7.485182989E+02	1.6557166E+02	9.500000E+00	2.500000E-01	39				
56	5.829466373E+02	1.2894734E+02	9.750000E+00	2.500000E-01	40				
57	4.539992976E+02	1.0042429E+02	1.000000E+01	2.500000E-01	41			22	
58	3.535750085E+02	7.8210515E+01	1.025000E+01	2.500000E-01	42				
59	2.753644935E+02	6.0910410E+01	1.050000E+01	2.500000E-01	43				
60	2.144540832E+02	4.7437075E+01	1.075000E+01	2.500000E-01	44				
61	1.670170079E+02	3.6944031E+01	1.100000E+01	2.500000E-01	45			23	
62	1.300729765E+02	2.8772040E+01	1.125000E+01	2.500000E-01	46				
63	1.013009360E+02	2.2407688E+01	1.150000E+01	2.500000E-01	47				
64	7.889324827E+01	5.2932483E+00	1.175000E+01	6.945063E-02	48				
65	7.360000000E+01	3.8500000E+00	1.181945E+01	5.372761E-02					
66	6.975000000E+01	1.2000000E+00	1.187318E+01	1.735401E-02					
67	6.855000000E+01	1.5500000E+00	1.189053E+01	2.287079E-02					
68	6.700000000E+01	5.5578765E+00	1.191340E+01	8.659697E-02					
69	6.144212353E+01	1.5421235E+00	1.200000E+01	2.541915E-02	49			24	
70	5.990000000E+01	8.5000000E-01	1.202542E+01	1.429196E-02					
71	5.905000000E+01	6.5000000E-01	1.203971E+01	1.106865E-02					
72	5.840000000E+01	1.0548826E+01	1.205078E+01	1.992202E-01					
73	4.785117392E+01	7.8511739E+00	1.225000E+01	1.792162E-01	50				
74	4.000000000E+01	2.7334683E+00	1.242922E+01	7.078380E-02					
75	3.726653172E+01	1.2165317E+00	1.250000E+01	3.318879E-02	51				
76	3.605000000E+01	1.0500000E+00	1.253319E+01	2.955880E-02					
77	3.500000000E+01	5.9767959E+00	1.256275E+01	1.872524E-01					
78	2.902320409E+01	5.3132041E+00	1.275000E+01	2.021988E-01	52				
79	2.371000000E+01	5.1000000E-01	1.295220E+01	2.174462E-02					
80	2.320000000E+01	5.9670593E-01	1.297394E+01	2.605663E-02					
81	2.260329407E+01	5.0329407E-01	1.300000E+01	2.251804E-02	53			25	

GROUP NO.	UPPER ENERGY BOUND,(EV)	GROUP ENERGY WIDTH,(EV)	LETHARGY	LETHARGY DIFFERENCE	CORRESPONDS WITH UPPER BOUND OF GROUPS IN THE FOLLOWING GAMI 68	GRANIT 48	LASER 35	LASL 30	EPRI 4
82	2.210000000E+01	6.0000000E-01	1.302252E+01	2.752467E-02					
83	2.150000000E+01	1.2000000E+00	1.305004E+01	5.743205E-02					
84	2.030000000E+01	2.6965369E+00	1.310747E+01	1.425252E-01					
85	1.760346312E+01	3.8938723E+00	1.325000E+01	2.500000E-01	54				
86	1.370959086E+01	3.0325508E+00	1.350000E+01	2.500000E-01	55				
87	1.067704010E+01	2.3617529E+00	1.375000E+01	2.500000E-01	56				
88	8.315287191E+00	1.3152872E+00	1.400000E+01	1.721855E-01	57			26	
89	7.000000000E+00	5.2404782E-01	1.417219E+01	7.781450E-02					
90	6.475952176E+00	1.4324755E+00	1.425000E+01	2.500000E-01	58				
91	5.043476626E+00	1.1156131E+00	1.450000E+01	2.500000E-01	59				
92	3.927863545E+00	8.6884034E-01	1.475000E+01	2.500000E-01	60				
93	3.059023205E+00	4.9817846E-01	1.500000E+01	1.777585E-01	61	48		27	
94	2.560844746E+00	1.7847508E-01	1.517776E+01	7.224153E-02		47			
95	2.382369668E+00	6.6344444E-02	1.525000E+01	2.824320E-02	62	46			
96	2.316025224E+00	2.1734124E-02	1.527824E+01	9.428544E-03		45			
97	2.294291100E+00	2.1631664E-02	1.528767E+01	9.473203E-03		44			
98	2.272659436E+00	2.1529203E-02	1.529714E+01	9.518288E-03		43			
99	2.251130233E+00	7.9001585E-02	1.530666E+01	3.572479E-02		42			
100	2.172128648E+00	7.8050829E-02	1.534239E+01	3.659436E-02		41			
101	2.094077819E+00	7.6170895E-02	1.537898E+01	3.705248E-02		40			
102	2.017906924E+00	8.2290918E-02	1.541603E+01	4.163517E-02		39			
103	1.935616006E+00	8.0224643E-02	1.545767E+01	4.232997E-02		38			
*104	1.855391363E+00	4.6423297E-02	1.550000E+01	2.533910E-02	63	37	35		
105	1.808968066E+00	4.5913180E-02	1.552534E+01	2.570852E-02		36			
106	1.763054886E+00	3.6974385E-02	1.555105E+01	2.119480E-02		35			
107	1.726080501E+00	8.3486240E-03	1.557224E+01	4.848487E-03			34		
108	1.717731877E+00	7.0146149E-02	1.557709E+01	4.169372E-02		34			
109	1.647585728E+00	5.2654518E-02	1.561878E+01	3.248041E-02		33			
110	1.594931210E+00	1.6429054E-02	1.565127E+01	1.035421E-02			33		
111	1.578502156E+00	1.2108290E-01	1.566162E+01	7.980916E-02		32			
112	1.457419257E+00	1.2439011E-02	1.574143E+01	8.571589E-03			32		
113	1.444980246E+00	1.3712785E-01	1.575000E+01	9.970925E-02	64	31			
114	1.307852396E+00	9.9180537E-02	1.584971E+01	7.886428E-02			31		
115	1.208671859E+00	4.2290688E-02	1.592857E+01	3.561618E-02		30			
116	1.166381171E+00	4.1029424E-02	1.596419E+01	3.581029E-02			30		
117	1.125351747E+00	2.6670325E-02	1.600000E+01	2.398490E-02	65			28	
118	1.098681422E+00	2.6513205E-02	1.602398E+01	2.442778E-02		29	29		
119	1.072168217E+00	9.8589660E-03	1.604841E+01	9.237892E-03		28	28		
120	1.062309251E+00	9.8134280E-03	1.605765E+01	9.280759E-03		27	27		
121	1.052495823E+00	9.7678900E-03	1.606693E+01	9.324026E-03		26	26		
122	1.042727933E+00	2.9030442E-02	1.607626E+01	2.823576E-02		25	25		
123	1.013697491E+00	6.3044759E-02	1.610449E+01	6.421097E-02		24	24		
124	9.506527323E-01	7.4227910E-02	1.616870E+01	8.129791E-02		23	23		

GROUP NO.	UPPER ENERGY BOUND,(EV)	GROUP ENERGY WIDTH,(EV)	LETHARGY	LETHARGY DIFFERENCE	CORRESPONDS WITH UPPER BOUND OF GROUPS IN THE FOLLOWING GAMI 68	GRANIT 48	LASER 35	LASL 30	EPRI 4
125	8.764248219E-01	9.4345983E-02	1.625000E+01	1.138954E-01	66				
126	7.820788385E-01	9.9518501E-02	1.636390E+01	1.361046E-01		22	22		
127	6.825603376E-01	5.7500338E-02	1.650000E+01	8.800328E-02	67				
*128	6.250600000E-01	9.3481475E-02	1.658800E+01	1.619967E-01		21	21		4
129	5.315785254E-01	2.8343722E-02	1.675000E+01	5.479406E-02	68				
130	5.032348036E-01	8.6218515E-02	1.680479E+01	1.879316E-01		20	20		
131	4.170162887E-01	3.0225168E-03	1.699273E+01	7.274353E-03		19	19		
*132	4.139937719E-01	5.6328609E-02	1.700000E+01	1.462537E-01	BOT			29	
133	3.576651631E-01	3.7037531E-02	1.714625E+01	1.093168E-01		18	18		
134	3.206276321E-01	1.9507951E-02	1.725557E+01	6.277263E-02		17	17		
135	3.011196812E-01	1.0382652E-02	1.731834E+01	3.508862E-02		16	16		
136	2.907370290E-01	2.0218849E-02	1.735343E+01	7.207987E-02		15	15		
137	2.705181801E-01	1.9490242E-02	1.742551E+01	7.477506E-02		14	14		
138	2.510279384E-01	2.3338198E-02	1.750029E+01	9.758033E-02		13	13		
139	2.276897400E-01	4.3261051E-02	1.759787E+01	2.107210E-01		12	12		
140	1.844286894E-01	3.2128892E-02	1.780859E+01	1.914120E-01		11	11		
141	1.522997974E-01	6.5783638E-03	1.800000E+01	4.415412E-02				30	
142	1.457214336E-01	3.4153461E-02	1.804415E+01	2.670628E-01		10	10		
143	1.115679726E-01	2.9599666E-02	1.831122E+01	3.083014E-01		9	9		
144	8.196830640E-02	2.5045871E-02	1.861952E+01	3.646431E-01		8	8		
145	5.692243500E-02	1.4167362E-02	1.898416E+01	2.862017E-01		7	7		
146	4.275507340E-02	1.2143453E-02	1.927036E+01	3.341082E-01		6	6		
147	3.061162060E-02	1.0119544E-02	1.960447E+01	4.013414E-01		5	5		
148	2.049207660E-02	8.0956352E-03	2.000581E+01	5.026289E-01		4	4		
149	1.239644140E-02	6.0717264E-03	2.050844E+01	6.729445E-01		3	3		
150	6.324715000E-03	4.0478176E-03	2.118139E+01	1.021651E+00		2	2		
151	2.276897400E-03	1.5166787E-03	2.220304E+01	1.096963E+00		1	1		
152	7.602187410E-04	5.0723014E-04	2.330000E+01	1.100262E+00					
153	2.529886000E-04	1.1410916E-04	2.440026E+01	5.997382E-01		BOT	BOT		
154	1.388794386E-04	1.2887944E-04	2.500000E+01	2.631021E+00				BOT	
LOWER BOUND	1.000000000E-05		2.763102E+01						

*THE UPPER ENERGY BOUNDRIES OF GROUPS 104,128 AND 132 CORRESPOND TO LETHARGY VALUES OF 15.5,16.588 AND 17.0 OF THE CSEWG 239-GROUP STRUCTURE. THESE ENERGIES DIFFER SLIGHTLY FROM THE VELOCITY-SPECIFIED BOUNDRIES OF GROUP STRUCTURES USED WITH GRANIT AND LASER.

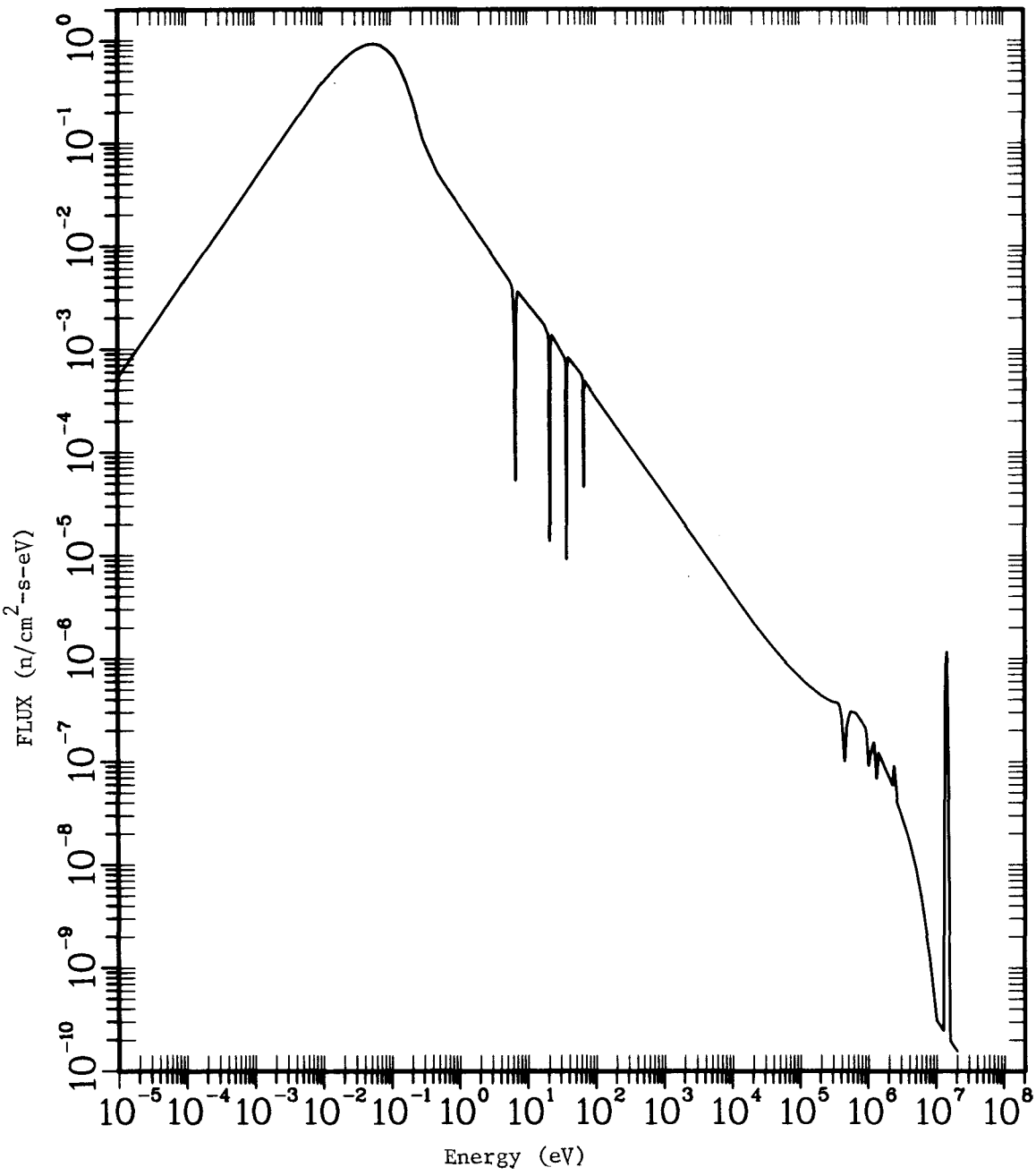

Fig. 4. PRS flux weighting function.

TABLE 3

PRS FLUX WEIGHTING FUNCTION

POINT	ENERGY, (EV)	FLUX	POINT	ENERGY, (EV)	FLUX	POINT	ENERGY, (EV)	FLUX
1	1.0000E-05	5.2500E-04	40	3.5600E+01	7.4897E-04	78	3.0000E+06	3.1142E-08
2	9.0000E-03	3.5500E-01	41	3.5900E+01	6.7872E-04	79	4.0000E+06	1.7073E-08
3	1.6000E-02	5.5200E-01	42	3.6700E+01	9.1595E-06	80	5.0000E+06	9.0679E-09
4	2.4000E-02	7.1200E-01	43	3.7400E+01	6.5453E-04	81	6.0000E+06	4.7153E-09
5	2.9000E-02	7.8500E-01	44	3.8700E+01	8.2618E-04	82	8.0000E+06	1.2276E-09
6	3.3000E-02	8.2900E-01	45	6.1200E+01	5.5873E-04	83	1.0000E+07	3.0953E-10
7	4.3000E-02	8.9800E-01	46	6.4900E+01	4.8243E-04	84	1.2570E+07	2.4619E-10
8	5.0000E-02	9.1800E-01	47	6.6000E+01	4.5797E-05	85	1.2600E+07	3.4731E-10
9	5.4000E-02	9.2100E-01	48	6.7100E+01	4.7226E-04	86	1.2700E+07	1.0357E-09
10	5.9000E-02	9.1800E-01	49	6.8200E+01	4.8362E-04	87	1.2800E+07	2.8436E-09
11	7.0000E-02	8.9200E-01	50	1.0100E+03	3.7829E-05	88	1.2900E+07	7.1910E-09
12	9.0000E-02	7.9900E-01	51	2.0000E+04	2.2257E-06	89	1.3000E+07	1.6776E-08
13	1.1200E-01	6.8600E-01	52	3.0700E+04	1.5571E-06	90	1.3100E+07	3.6122E-08
14	1.4000E-01	5.2000E-01	53	6.0700E+04	9.1595E-07	91	1.3200E+07	7.1864E-08
15	1.7000E-01	3.8300E-01	54	1.2000E+05	5.7934E-07	92	1.3300E+07	1.3222E-07
16	2.1000E-01	2.5200E-01	55	2.0100E+05	4.3645E-07	93	1.3400E+07	2.2511E-07
17	3.0000E-01	1.0800E-01	56	2.8300E+05	3.8309E-07	94	1.3500E+07	3.5512E-07
18	4.0000E-01	6.8700E-02	57	3.5600E+05	3.6926E-07	95	1.3600E+07	5.1946E-07
19	4.9000E-01	5.1000E-02	58	3.7700E+05	3.4027E-07	96	1.3700E+07	7.0478E-07
20	5.7000E-01	4.3700E-02	59	3.9900E+05	2.7387E-07	97	1.3800E+07	8.8825E-07
21	6.0000E-01	4.1300E-02	60	4.4200E+05	1.0075E-07	98	1.3900E+07	1.0408E-06
22	1.0000E+00	2.4914E-02	61	4.7400E+05	2.1754E-07	99	1.4070E+07	1.1540E-06
23	1.3518E+00	1.8502E-02	62	5.0200E+05	2.6333E-07	100	1.4200E+07	1.0870E-06
24	4.0100E+00	6.3200E-03	63	5.4000E+05	3.0501E-07	101	1.4300E+07	9.5757E-07
25	5.5047E+00	4.6164E-03	64	6.5000E+05	2.9493E-07	102	1.4400E+07	7.8704E-07
26	5.8842E+00	4.1950E-03	65	7.7000E+05	2.5005E-07	103	1.4500E+07	6.0403E-07
27	6.1350E+00	3.7279E-03	66	9.0000E+05	2.1479E-07	104	1.4600E+07	4.3317E-07
28	6.4490E+00	1.6524E-03	67	9.4100E+05	1.7861E-07	105	1.4700E+07	2.9041E-07
29	6.6700E+00	5.3125E-05	68	1.0000E+06	9.1595E-08	106	1.4800E+07	1.8213E-07
30	6.8940E+00	1.7632E-03	69	1.0500E+06	1.1518E-07	107	1.4900E+07	1.0699E-07
31	7.0100E+00	2.9219E-03	70	1.1200E+06	1.3648E-07	108	1.5000E+07	5.8832E-08
32	7.3080E+00	3.6042E-03	71	1.1900E+06	1.5479E-07	109	1.5100E+07	3.0354E-08
33	1.7530E+01	1.7156E-03	72	1.2100E+06	1.5022E-07	110	1.5200E+07	1.4687E-08
34	1.9860E+01	1.3858E-03	73	1.3100E+06	6.8696E-08	111	1.5300E+07	6.6688E-09
35	2.0370E+01	1.0973E-03	74	1.4000E+06	1.2182E-07	112	1.5400E+07	2.8450E-09
36	2.0900E+01	1.3739E-05	75	2.2200E+06	5.9033E-08	113	1.5500E+07	1.1406E-09
37	2.1400E+01	1.0588E-03	76	2.3500E+06	9.1595E-08	114	1.5676E+07	1.9780E-10
38	2.2500E+01	1.3565E-03	77	2.6300E+06	3.9981E-08	115	2.0000E+07	1.5477E-10
39	3.4400E+01	8.1519E-04						

FLUX VALUES ARE GIVEN IN UNITS OF NEUTRONS/ CM**2 SEC. EV.

subsequently collapsed to the EPRI Four-Group Structure, using the TOAFEW[10] collapsing code. Without exception, fission-product neutron absorption cross sections other than radiative capture were observed to be negligible within the scope of this work. The higher temperature radiative capture (MT=102) 4-group cross sections are listed in Table 4.

In addition to 4-group cross sections, Table 4 also lists effective thermal cross section values. This parameter, discussed in Sec. 6 and in Sec. 1 of Part 2 of this report, is the ratio of the group 4 flux-weighted average cross section to the group 4 flux-weighted average of a cross section equal to unity at 2200 m/s and having a 1/v dependence. Thus, the effective thermal cross section would be the 2200 m/s value of a truly 1/v cross section.

Not all of the 181 nuclei having evaluated cross sections are among the 186 nuclei included in the EPRI-CINDER chain structure. Some 28 of the nuclei in the chain structure have no evaluated cross sections in ENDF/B-IV. Only 1, $^{79}_{34}Se$, appears in absorption coupling. The 4-group cross-section values used for $^{79}_{34}Se$ were taken from previous CINDER libraries. The remaining 27 nuclei have short half-lives and were assigned cross-section values of zero; these therefore affect only transient absorption or the rate of absorption buildup.

All branching fractions for competing radioactive decay and absorption reactions were taken from Ref. 5. In some instances, effective branching fractions were formulated to accomodate the branching to and from short-lived nuclei or metastable states not explicitly included in the EPRI-CINDER chain structure. Radioactive decay constants were computed from half-lives given in Ref. 5.

Decay constants, four-group radiative capture cross sections, and branching fractions were combined with chain parameters, using the NKDECK[10] program, to produce the chain nuclide cards for the data set.

Yield Data

The YLDECK[10] program was used to compute effective fission yield fraction values for all nuclei in the chain structure and, with input chain parameters, to produce the yield cards for the data set.

TABLE 4

FOUR GROUP CROSS SECTIONS

NUCLIDE	Z	A	S	MT NO	MAT NO	TEMP DEG.KEL	SIGMA ZERO	GROUP 1 CROSS SECTION	GROUP 2 CROSS SECTION	GROUP 3 CROSS SECTION	GROUP 4 CROSS SECTION	EFFECTIVE THERMAL CROSS SECTION
GE072	32	72	0	102	48	1.0E+03	1.0E+10	2.099716E-02	5.432289E-02	8.043696E-02	5.476937E-01	9.885840E-01
GE073	32	73	0	102	49	1.0E+03	1.0E+10	4.379093E-02	1.769910E-01	8.051782E+00	8.381628E+00	1.512879E+01
GE074	32	74	0	102	51	1.0E+03	1.0E+10	9.484258E-03	3.185640E-02	4.402824E-02	2.141804E-01	3.865945E-01
GE076	32	76	0	102	54	1.0E+03	1.0E+10	2.668907E-03	9.284226E-03	1.632492E-01	7.941654E-02	1.433464E-01
AS075	33	75	0	102	68	1.0E+03	1.0E+10	3.174023E-02	2.399267E-01	7.066404E+00	2.408837E+00	4.347936E+00
SE076	34	76	0	102	85	1.0E+03	1.0E+10	3.043571E-02	1.025647E-01	3.876426E+00	4.754810E+01	8.582406E+01
SE077	34	77	0	102	86	1.0E+03	1.0E+10	2.397912E-02	2.570206E-01	3.571884E+00	2.346095E+01	4.234688E+01
SE078	34	78	0	102	88	1.0E+03	1.0E+10	1.233979E-02	4.559968E-02	5.350889E-01	2.234162E-01	4.032650E-01
SE080	34	80	0	102	91	1.0E+03	1.0E+10	1.224080E-02	4.557911E-02	8.982662E-02	3.412236E-01	6.159067E-01
SE082	34	82	0	102	94	1.0E+03	1.0E+10	3.747510E-03	1.079513E-02	1.686126E-03	2.513117E-02	4.536163E-02
BR079	35	79	0	102	108	1.0E+03	1.0E+10	6.182080E-02	4.360678E-01	1.200472E+01	6.222752E+00	1.123203E+01
BR081	35	81	0	102	112	1.0E+03	1.0E+10	4.217740E-02	2.809681E-01	5.719193E+00	1.503798E+00	2.714348E+00
KR080	36	80	0	102	131	1.0E+03	1.0E+10	3.268930E-02	1.358841E-01	6.958419E+00	7.974773E+00	1.439442E+01
KR082	36	82	0	102	134	1.0E+03	1.0E+10	3.209819E-02	1.243721E-01	1.984202E+01	1.685921E+01	3.043078E+01
KR083	36	83	0	102	135	1.0E+03	1.0E+10	6.710060E-02	3.993954E-01	1.841473E+01	1.119001E+02	2.019790E+02
KR084	36	84	0	102	137	1.0E+03	1.0E+10	4.472712E-03	1.912670E-02	4.376474E-01	4.633101E-02	8.362721E-02
KR085	36	85	0	102	138	1.0E+03	1.0E+10	4.363354E-03	2.864559E-02	1.600506E-01	9.295652E-01	1.677860E+00
KR086	36	86	0	102	140	1.0E+03	1.0E+10	1.108820E-03	3.162755E-03	1.545394E-02	3.441791E-02	6.212414E-02
RB085	37	85	0	102	153	1.0E+03	1.0E+10	2.080914E-02	2.157803E-01	5.395468E-01	2.576161E-01	4.649955E-01
RB086	37	86	0	102	154	1.0E+03	1.0E+10	4.296598E-03	9.237312E-02	2.813636E+00	2.735252E+00	4.937115E+00
RB087	37	87	0	102	156	1.0E+03	1.0E+10	1.287127E-03	8.266649E-03	2.536605E-01	6.710316E-02	1.211208E-01
SR086	38	86	0	102	172	1.0E+03	1.0E+10	1.688432E-02	4.158945E-02	5.748211E-01	1.588873E+00	2.867907E+00
SR087	38	87	0	102	173	1.0E+03	1.0E+10	1.669480E-02	7.775602E-02	1.045327E+01	9.270864E+00	1.673386E+01
SR088	38	88	0	102	175	1.0E+03	1.0E+10	1.329117E-03	1.164227E-03	2.201289E-04	3.248619E-03	5.863738E-03
SR089	38	89	0	102	176	1.0E+03	1.0E+10	8.295338E-03	2.038847E-02	3.876896E-02	2.348515E-01	4.239056E-01
SR090	38	90	0	102	177	1.0E+03	1.0E+10	4.920037E-03	1.560162E-02	3.315065E-02	5.026414E-01	9.072648E-01
Y089	39	89	0	102	192	1.0E+03	1.0E+10	7.136131E-03	2.253723E-02	8.228017E-02	7.165644E-01	1.293395E+00
Y090	39	90	0	102	194	1.0E+03	1.0E+10	1.138581E-02	1.146555E-01	4.323381E-01	1.954493E+00	3.527849E+00
Y091	39	91	0	102	196	1.0E+03	1.0E+10	4.217073E-03	3.284697E-02	1.639328E-01	7.827059E-01	1.412780E+00
ZR090	40	90	0	102	215	1.0E+03	1.0E+10	1.508096E-02	2.520652E-02	1.987868E-02	5.586877E-02	1.008428E-01
ZR091	40	91	0	102	217	1.0E+03	1.0E+10	1.715130E-02	5.507396E-02	6.700606E-01	5.758814E-01	1.039463E+00
ZR092	40	92	0	102	218	1.0E+03	1.0E+10	1.042367E-02	3.130879E-02	8.308115E-02	1.452876E-01	2.622433E-01
ZR093	40	93	0	102	219	1.0E+03	1.0E+10	2.089521E-02	5.150402E-02	3.654891E+00	1.396955E+00	2.521495E+00
ZR094	40	94	0	102	220	1.0E+03	1.0E+10	5.447404E-03	2.595021E-02	2.019570E-02	3.128906E-02	5.647657E-02
ZR095	40	95	0	102	221	1.0E+03	1.0E+10	3.771503E-02	1.168058E-01	5.797035E-01	2.741127E-01	4.947719E-01
ZR096	40	96	0	102	222	1.0E+03	1.0E+10	2.648158E-02	2.165040E-02	6.357653E-01	8.862928E-03	1.599754E-02
NB093	41	93	0	102	1189	9.0E+02	1.0E+10	1.604464E-02	1.581963E-01	1.036643E+00	6.392347E-01	1.153815E+00
NB094	41	94	0	102	238	1.0E+03	1.0E+10	5.739899E-03	1.688129E-01	1.173435E+01	7.640611E+00	1.379126E+01
NB095	41	95	0	102	240	1.0E+03	1.0E+10	5.266054E-02	2.650329E-01	2.503124E+00	8.380113E-01	1.512606E+00
MO094	42	94	0	102	264	1.0E+03	1.0E+10	1.622583E-02	3.166593E-02	9.483319E-02	8.925915E-03	1.611123E-02
MO095	42	95	0	102	265	1.0E+03	1.0E+10	3.417280E-02	2.320601E-01	1.257062E+01	8.099988E+00	1.462043E+01
MO096	42	96	0	102	266	1.0E+03	1.0E+10	1.622694E-02	4.895069E-02	2.259064E+00	5.590317E-01	1.009049E+00

NUCLIDE	Z	A	S	MT NO	MAT NO	TEMP DEG.KEL	SIGMA ZERO	GROUP 1 CROSS SECTION	GROUP 2 CROSS SECTION	GROUP 3 CROSS SECTION	GROUP 4 CROSS SECTION	EFFECTIVE THERMAL GROSS SECTION
MO097	42	97	0	102	267	1.0E+03	1.0E+10	2.907559E-02	2.248807E-01	1.719731E+00	1.215824E+00	2.194556E+00
MO098	42	98	0	102	268	1.0E+03	1.0E+10	2.516355E-02	7.168378E-02	7.678803E-01	7.125803E-02	1.286203E-01
MO099	42	99	0	102	269	1.0E+03	1.0E+10	4.286153E-02	4.063070E-01	2.849176E+00	9.492203E-01	1.713337E+00
MO100	42	100	0	102	270	1.0E+03	1.0E+10	9.074271E-03	5.494819E-02	4.423330E-01	1.111105E-01	2.005538E-01
TC099	43	99	0	102	1137	9.0E+02	1.0E+10	3.673952E-02	3.614800E-01	3.069278E+01	1.083246E+01	1.955253E+01
RU099	44	99	0	102	308	1.0E+03	1.0E+10	3.826665E-02	3.753455E-01	1.421606E+01	2.833373E+00	5.114222E+00
RU100	44	100	0	102	309	1.0E+03	1.0E+10	3.858774E-02	1.136596E-01	1.132016E+00	3.239899E+00	5.847999E+00
RU101	44	101	0	102	310	1.0E+03	1.0E+10	2.690347E-02	4.480972E-01	9.421788E+00	1.743797E+00	3.147543E+00
RU102	44	102	0	102	311	1.0E+03	1.0E+10	6.954545E-02	1.577507E-01	3.499625E-01	7.279318E-01	1.313913E+00
RU103	44	103	0	102	312	1.0E+03	1.0E+10	2.468305E-02	3.671989E-01	7.404899E+00	4.301005E+00	7.763290E+00
RU104	44	104	0	102	313	1.0E+03	1.0E+10	3.070218E-02	1.059028E-01	7.196752E-01	2.440178E-01	4.404508E-01
RU105	44	105	0	102	314	1.0E+03	1.0E+10	2.325016E-02	3.233188E-01	6.399468E-01	1.117743E-01	2.017520E-01
RU106	44	106	0	102	315	1.0E+03	1.0E+10	8.344953E-03	5.233636E-02	2.475373E-01	8.153410E-02	1.471686E-01
RH103	45	103	0	102	1125	9.0E+02	1.0E+10	4.648621E-02	5.571160E-01	9.047802E+01	9.701271E+01	1.751074E+02
RH105	45	105	0	102	334	1.0E+03	1.0E+10	9.125643E-02	4.919683E-01	7.002262E+02	4.934551E+03	8.906837E+03
PD104	46	104	0	102	358	1.0E+03	1.0E+10	8.530148E-02	2.169388E-01	2.016123E+00	2.166387E-01	3.910315E-01
PD105	46	105	0	102	359	1.0E+03	1.0E+10	8.900761E-02	7.121473E-01	9.287985E+00	7.843382E+00	1.415726E+01
PD106	46	106	0	102	360	1.0E+03	1.0E+10	4.789705E-02	1.283831E-01	7.720379E-01	1.332195E-01	2.404604E-01
PD107	46	107	0	102	361	1.0E+03	1.0E+10	6.726203E-02	4.894277E-01	7.143654E+00	5.588543E+00	1.008729E+01
PD108	46	108	0	102	363	1.0E+03	1.0E+10	4.149806E-02	1.255796E-01	2.259456E+01	6.845444E+00	1.235599E+01
PD110	46	110	0	102	366	1.0E+03	1.0E+10	1.580939E-02	7.311286E-02	8.358860E-01	1.229825E-01	2.219828E-01
AG107	47	107	0	102	1138	9.0E+02	1.0E+10	8.334117E-02	5.664923E-01	1.210986E+01	2.047736E+01	3.696153E+01
AG109	47	109	0	102	1139	9.0E+02	1.0E+10	4.458553E-02	3.535820E-01	1.302363E+02	5.257063E+01	9.488969E+01
AG111	47	111	0	102	391	1.0E+03	1.0E+10	2.611568E-02	3.334252E-01	1.231271E+01	1.677295E+00	3.027507E+00
CD108	48	108	0	102	415	1.0E+03	1.0E+10	9.591343E-02	1.805074E-01	3.702015E-01	6.153806E-01	1.110758E+00
CD110	48	110	0	102	417	1.0E+03	1.0E+10	1.158785E-01	2.033491E-01	4.663889E+00	6.207640E+00	1.120475E+01
CD111	48	111	0	102	418	1.0E+03	1.0E+10	3.549300E-02	3.246907E-01	5.577368E+00	1.357310E+01	2.449936E+01
CD112	48	112	0	102	420	1.0E+03	1.0E+10	9.319133E-02	1.924481E-01	1.147311E+00	1.230079E+00	2.220285E+00
CD113	48	113	0	102	1282	9.0E+02	1.0E+10	4.035980E-02	2.936839E-01	2.050547E+01	2.727591E+04	4.923287E+04
CD114	48	114	0	102	423	1.0E+03	1.0E+10	9.644373E-02	2.058760E-01	2.208012E+00	1.877895E-01	3.389589E-01
CD15M	48	115	1	102	425	1.0E+03	1.0E+10	3.428619E-02	2.347852E-01	2.2264[illegible]9E+01	1.732369E+01	3.126916E+01
CD116	48	116	0	102	426	1.0E+03	1.0E+10	4.177477E-02	9.279391E-02	2.235261E-01	4.293487E-02	7.749719E-02
IN113	49	113	0	102	445	1.0E+03	1.0E+10	2.409397E-01	5.236885E-01	2.162369E+01	6.590786E+00	1.189633E+01
IN115	49	115	0	102	449	1.0E+03	1.0E+10	1.228192E-01	3.755484E-01	2.854463E+02	1.289674E+02	2.327855E+02
SN115	50	115	0	102	482	1.0E+03	1.0E+10	3.729064E-03	3.183642E-02	2.008304E+00	2.796581E+01	5.047812E+01
SN116	50	116	0	102	483	1.0E+03	1.0E+10	3.175388E-02	4.364059E-02	1.356454E+00	6.732990E-02	1.215301E-01
SN117	50	117	0	102	484	1.0E+03	1.0E+10	3.274490E-02	1.661797E-01	1.984944E+00	1.455753E+00	2.627627E+00
SN118	50	118	0	102	486	1.0E+03	1.0E+10	7.690040E-02	8.667272E-02	6.911670E-01	4.610512E-02	8.321948E-02
SN119	50	119	0	102	487	1.0E+03	1.0E+10	6.371977E-03	4.040596E-02	3.974212E-01	1.284014E+00	2.317637E+00
SN120	50	120	0	102	489	1.0E+03	1.0E+10	1.800320E-02	2.933619E-02	1.337315E-01	7.881781E-02	1.422657E-01
SN122	50	122	0	102	492	1.0E+03	1.0E+10	1.337318E-02	1.827124E-02	7.595520E-02	1.010517E-01	1.823978E-01
SN123	50	123	0	102	493	1.0E+03	1.0E+10	3.947307E-02	8.523844E-02	2.774607E-01	1.845241E-02	3.330650E-02
SN124	50	124	0	102	495	1.0E+03	1.0E+10	1.849913E-02	2.415400E-02	8.102987E-01	7.272250E-02	1.312637E-01
SN125	50	125	0	102	496	1.0E+03	1.0E+10	9.919385E-03	4.686948E-02	1.984130E+00	3.074827E-01	5.550044E-01
SN126	50	126	0	102	498	1.0E+03	1.0E+10	5.678309E-03	7.303296E-03	1.098527E-02	1.677718E-01	3.028272E-01
SB121	51	121	0	102	511	1.0E+03	1.0E+10	1.106325E-01	4.009508E-01	1.677825E+01	3.560680E+00	6.427007E+00
SB123	51	123	0	102	514	1.0E+03	1.0E+10	5.059958E-02	2.100477E-01	8.328224E+00	2.434903E+00	4.394987E+00

NUCLIDE	Z	A	S	MT NO	MAT NO	TEMP DEG.KEL	SIGMA ZERO	GROUP 1 CROSS SECTION	GROUP 2 CROSS SECTION	GROUP 3 CROSS SECTION	GROUP 4 CROSS SECTION	EFFECTIVE THERMAL CROSS SECTION
SB124	51	124	0	102	515	1.0E+03	1.0E+10	2.543705E-02	5.863286E-01	2.475458E+00	3.630309E+00	6.552687E+00
SB125	51	125	0	102	518	1.0E+03	1.0E+10	7.517359E-02	2.103150E-01	2.103414E+00	5.592590E-01	1.009459E+00
SB126	51	126	0	102	519	1.0E+03	1.0E+10	1.848180E-02	3.033790E-01	5.136429E+00	3.247778E+00	5.862222E+00
TE122	52	122	0	102	538	1.0E+03	1.0E+10	1.202321E-01	2.504961E-01	8.412152E+00	1.569423E+00	2.832800E+00
TE123	52	123	0	102	539	1.0E+03	1.0E+10	6.157976E-02	3.666051E-01	4.865476E+02	2.468661E+02	4.455918E+02
TE124	52	124	0	102	541	1.0E+03	1.0E+10	1.104859E-01	1.937552E-01	7.708467E-01	3.808186E+00	6.873755E+00
TE125	52	125	0	102	542	1.0E+03	1.0E+10	2.613155E-02	2.557467E-01	2.647459E+00	8.658353E-01	1.562828E+00
TE126	52	126	0	102	544	1.0E+03	1.0E+10	3.714886E-02	8.357152E-02	1.185596E+00	5.779812E-01	1.043253E+00
TE27M	52	127	1	102	546	1.0E+03	1.0E+10	5.419348E-02	2.648949E-01	4.726406E+00	5.264135E+00	9.501734E+00
TE128	52	128	0	102	547	1.0E+03	1.0E+10	4.529906E-02	8.662364E-02	2.271823E-01	1.202259E-01	2.170070E-01
TE29M	52	129	1	102	549	1.0E+03	1.0E+10	9.472597E-03	8.205984E-02	6.885660E-01	6.142364E-01	1.108693E+00
TE130	52	130	0	102	550	1.0E+03	1.0E+10	3.760774E-03	1.329507E-02	2.826283E-02	1.621755E-01	2.927259E-01
TE132	52	132	0	102	553	1.0E+03	1.0E+10	5.710111E-04	4.443987E-04	7.327881E-05	1.117629E-03	2.017314E-03
I127	53	127	0	102	565	1.0E+03	1.0E+10	5.610752E-02	3.939301E-01	1.539254E+01	3.478504E+00	6.278681E+00
I129	53	129	0	102	567	1.0E+03	1.0E+10	4.800948E-02	2.804701E-01	3.709139E+00	1.510053E+01	2.725637E+01
I130	53	130	0	102	568	1.0E+03	1.0E+10	1.837486E-02	2.696179E-01	1.985659E+01	1.004999E+01	1.814018E+01
I131	53	131	0	102	570	1.0E+03	1.0E+10	9.472026E-03	7.367629E-02	9.685281E-01	3.911037E-01	7.059400E-01
I135	53	135	0	102	576	1.0E+03	1.0E+10	4.684394E-04	5.736313E-04	7.324264E-04	1.118905E-02	2.019617E-02
XE128	54	128	0	102	1173	9.0E+02	1.0E+10	5.312305E-02	2.997089E-01	2.526227E+01	9.969592E+00	1.799506E+01
XE129	54	129	0	102	589	1.0E+03	1.0E+10	5.323277E-02	3.033197E-01	2.522329E+01	1.003302E+01	1.810954E+01
XE130	54	130	0	102	1174	9.0E+02	1.0E+10	3.404525E-02	1.127239E-01	3.154451E-01	3.446107E+00	6.220203E+00
XE131	54	131	0	102	1175	9.0E+02	1.0E+10	1.332154E-02	1.837029E-01	8.832394E+01	5.042924E+01	9.102450E+01
XE132	54	132	0	102	1176	9.0E+02	1.0E+10	1.814070E-02	6.651676E-02	1.568604E-01	2.501073E-01	4.514423E-01
XE133	54	133	0	102	595	1.0E+03	1.0E+10	5.950709E-03	5.286344E-02	3.435562E+01	1.062848E+02	1.918434E+02
XE134	54	134	0	102	1177	9.0E+02	1.0E+10	1.054011E-02	3.432525E-02	3.981692E-02	1.434189E-01	2.588703E-01
XE135	54	135	0	102	1294	9.0E+02	1.0E+10	5.564618E-04	3.218521E-03	3.634285E+02	1.670657E+06	3.015526E+06
XE136	54	136	0	102	1178	9.0E+02	1.0E+10	1.072229E-03	2.288886E-03	1.069663E-02	8.874087E-02	1.601768E-01
CS133	55	133	0	102	1141	9.0E+02	1.0E+10	5.103384E-02	3.777516E-01	3.378401E+01	1.663776E+01	3.003107E+01
CS134	55	134	0	102	614	1.0E+03	1.0E+10	1.286883E-02	3.448577E-01	2.079022E+01	7.828318E+01	1.413007E+02
CS135	55	135	0	102	616	1.0E+03	1.0E+10	3.180215E-03	4.148685E-02	4.381765E+00	4.866696E+00	8.784359E+00
CS136	55	136	0	102	618	1.0E+03	1.0E+10	1.942282E-02	1.635070E-01	3.303652E+00	7.287809E-01	1.315445E+00
CS137	55	137	0	102	619	1.0E+03	1.0E+10	1.502562E-03	5.543158E-03	5.867613E-02	6.142019E-02	1.108631E-01
BA134	56	134	0	102	634	1.0E+03	1.0E+10	3.524396E-02	8.612855E-02	2.724576E+00	1.205309E+00	2.175576E+00
BA135	56	135	0	102	635	1.0E+03	1.0E+10	2.867491E-02	2.214519E-01	1.119982E+01	3.250888E+00	5.867834E+00
BA136	56	136	0	102	637	1.0E+03	1.0E+10	1.312605E-02	3.583927E-02	2.133971E-01	2.289892E-01	4.133242E-01
BA137	56	137	0	102	639	1.0E+03	1.0E+10	7.225130E-03	3.743974E-02	4.969716E-01	2.849852E+00	5.143966E+00
BA138	56	138	0	102	641	1.0E+03	1.0E+10	9.214468E-03	5.529264E-03	1.282347E-02	1.955539E-01	3.529736E-01
BA140	56	140	0	102	643	1.0E+03	1.0E+10	1.689069E-03	3.743996E-03	1.567531E+00	8.912482E-01	1.608698E+00
LA139	57	139	0	102	657	1.0E+03	1.0E+10	6.009337E-03	2.967405E-02	1.244460E+00	5.013105E+00	9.048625E+00
LA140	57	140	0	102	658	1.0E+03	1.0E+10	2.948971E-02	1.295762E-01	7.885135E+00	1.508462E+00	2.722765E+00
CE140	58	140	0	102	674	1.0E+03	1.0E+10	1.703531E-02	1.730715E-02	2.903654E-02	3.190750E-01	5.759285E-01
CE141	58	141	0	102	675	1.0E+03	1.0E+10	4.510816E-02	1.054578E-01	2.342997E+00	1.619745E+01	2.923631E+01
CE142	58	142	0	102	676	1.0E+03	1.0E+10	1.485239E-02	3.294434E-02	5.925282E-02	5.307171E-01	9.579413E-01
CE143	58	143	0	102	677	1.0E+03	1.0E+10	9.577707E-03	7.577132E-02	5.095466E+00	3.349870E+00	6.046496E+00
CE144	58	144	0	102	678	1.0E+03	1.0E+10	1.090923E-02	2.405806E-02	2.314846E-01	5.586255E-01	1.008316E+00
PR141	59	141	0	102	692	1.0E+03	1.0E+10	2.548600E-02	9.959114E-02	2.105239E+00	6.439460E+00	1.162319E+01
PR142	59	142	0	102	693	1.0E+03	1.0E+10	1.604911E-02	2.547188E-01	1.527271E+01	1.117627E+01	2.017310E+01

NUCLIDE	Z	A	S	MT NO	MAT NO	TEMP DEG.KEL	SIGMA ZERO	GROUP 1 CROSS SECTION	GROUP 2 CROSS SECTION	GROUP 3 CROSS SECTION	GROUP 4 CROSS SECTION	EFFECTIVE THERMAL CROSS SECTION
PR143	59	143	0	102	695	1.0E+03	1.0E+10	4.842014E-02	2.161496E-01	1.913981E+01	4.977789E+01	8.984881E+01
ND142	60	142	0	102	713	1.0E+03	1.0E+10	2.773231E-02	3.127668E-02	7.312854E-01	1.044265E+01	1.884892E+01
ND143	60	143	0	102	714	1.0E+03	1.0E+10	5.923333E-02	1.938598E-01	1.209111E+01	1.773106E+02	3.200445E+02
ND144	60	144	0	102	715	1.0E+03	1.0E+10	4.188978E-02	6.863372E-02	5.867006E-01	2.013982E+00	3.635226E+00
ND145	60	145	0	102	716	1.0E+03	1.0E+10	6.803414E-02	1.983824E-01	2.256161E+01	2.355985E+01	4.252540E+01
ND146	60	146	0	102	717	1.0E+03	1.0E+10	5.710881E-02	1.082823E-01	2.963151E-01	7.827704E-01	1.412896E+00
ND147	60	147	0	102	718	1.0E+03	1.0E+10	5.106341E-02	3.928675E-01	6.013407E+01	2.740049E+01	4.945773E+01
ND148	60	148	0	102	719	1.0E+03	1.0E+10	1.435365E-01	1.318842E-01	2.284639E+00	1.399507E+00	2.526102E+00
ND150	60	150	0	102	721	1.0E+03	1.0E+10	5.230297E-02	1.742186E-01	1.865556E+00	6.713311E-01	1.211749E+00
PM147	61	147	0	102	733	1.0E+03	1.0E+10	1.382808E-01	8.170927E-01	1.918335E+02	9.917021E+01	1.790017E+02
PM148	61	148	0	102	734	1.0E+03	1.0E+10	4.921928E-01	2.574234E+00	2.332976E+03	2.594150E+03	4.682426E+03
PM48M	61	148	1	102	735	1.0E+03	1.0E+10	4.921928E-01	2.574234E+00	3.182157E+02	1.909160E+04	3.446023E+04
PM149	61	149	0	102	736	1.0E+03	1.0E+10	5.268164E-01	2.133433E+00	7.332632E+01	7.811904E+02	1.410044E+03
PM151	61	151	0	102	738	1.0E+03	1.0E+10	1.012214E-03	2.037358E-02	1.742050E+02	3.910634E+02	7.058672E+02
SM147	62	147	0	102	753	1.0E+03	1.0E+10	1.180276E-01	5.432755E-01	7.514796E+01	3.454724E+01	6.235757E+01
SM148	62	148	0	102	754	1.0E+03	1.0E+10	2.023254E-01	2.596780E-01	3.134887E+00	1.509450E+00	2.724549E+00
SM149	62	149	0	102	1027	9.0E+02	1.0E+10	5.637011E-02	9.344686E-01	2.770684E+02	4.841072E+04	8.738108E+04
SM150	62	150	0	102	756	1.0E+03	1.0E+10	1.313093E-01	2.862238E-01	1.160902E+01	5.471646E+01	9.876290E+01
SM151	62	151	0	102	757	1.0E+03	1.0E+10	2.315641E-01	1.356167E+00	2.894601E+02	4.669738E+03	8.428850E+03
SM152	62	152	0	102	758	1.0E+03	1.0E+10	7.520442E-02	2.877061E-01	2.755117E+02	1.173567E+02	2.118281E+02
SM153	62	153	0	102	759	1.0E+03	1.0E+10	2.260670E-04	1.191724E-02	2.418654E+02	1.846696E+02	3.333276E+02
SM154	62	154	0	102	760	1.0E+03	1.0E+10	5.706727E-02	1.425114E-01	3.851160E+00	3.076205E+00	5.552533E+00
EU151	63	151	0	102	1290	9.0E+02	1.0E+10	4.181577E-01	2.402754E+00	2.044278E+02	4.717469E+03	8.515005E+03
EU152	63	152	0	102	1292	9.0E+02	1.0E+10	1.744222E-01	3.245252E+00	3.252586E+02	7.677840E+02	1.385846E+03
EU153	63	153	0	102	1291	9.0E+02	1.0E+10	2.431446E-01	1.539698E+00	1.478631E+02	2.197333E+02	3.966174E+02
EU154	63	154	0	102	1293	9.0E+02	1.0E+10	7.241066E-02	1.875663E+00	2.228416E+02	4.972313E+02	8.974997E+02
EU155	63	155	0	102	778	1.0E+03	1.0E+10	9.062116E-01	1.543263E+00	1.540107E+02	2.258836E+03	4.077187E+03
EU156	63	156	0	102	779	1.0E+03	1.0E+10	5.008924E-04	3.539738E-02	1.016701E+02	2.696344E+02	4.866885E+02
EU157	63	157	0	102	780	1.0E+03	1.0E+10	3.221641E-03	2.526199E-02	8.471598E+01	1.059332E+02	1.912089E+02
GD154	64	154	0	102	791	1.0E+03	1.0E+10	3.041554E-01	6.280531E-01	2.531751E+01	4.755081E+01	8.582895E+01
GD155	64	155	0	102	792	1.0E+03	1.0E+10	1.251320E-01	1.467746E+00	1.313204E+02	1.920502E+04	3.466494E+04
GD156	64	156	0	102	793	1.0E+03	1.0E+10	1.177736E-01	2.925910E-01	1.328447E+01	8.292483E-01	1.496788E+00
GD157	64	157	0	102	794	1.0E+03	1.0E+10	1.068337E-01	7.103253E-01	8.871128E+01	8.261695E+04	1.491231E+05
GD158	64	158	0	102	795	1.0E+03	1.0E+10	4.647452E-02	1.882511E-01	6.519250E+00	1.403779E+00	2.533814E+00
GD160	64	160	0	102	797	1.0E+03	1.0E+10	8.083934E-02	1.503781E-01	9.311768E-01	4.300564E-01	7.762493E-01
TB159	65	159	0	102	803	1.0E+03	1.0E+10	9.138282E-02	7.922879E-01	4.634842E+01	1.437843E+01	2.595299E+01
TB160	65	160	0	102	804	1.0E+03	1.0E+10	1.434563E-03	7.845290E-02	8.018238E+01	2.928139E+02	5.285275E+02
DY160	66	160	0	102	811	1.0E+03	1.0E+10	7.939346E-01	1.200462E+00	1.508596E+02	3.609387E+01	6.514924E+01
DY161	66	161	0	102	812	1.0E+03	1.0E+10	5.945760E-02	1.227134E+00	1.166236E+02	3.112586E+02	5.618201E+02
DY162	66	162	0	102	813	1.0E+03	1.0E+10	2.803023E-01	5.297747E-01	2.471440E+02	1.147570E+02	2.071357E+02
DY163	66	163	0	102	814	1.0E+03	1.0E+10	5.480996E-02	5.190151E-01	1.336405E+02	7.776202E+01	1.403600E+02
DY164	66	164	0	102	1031	9.0E+02	1.0E+10	9.006775E-02	1.915334E-01	2.300536E+01	1.300572E+03	2.347525E+03
HO165	67	165	0	102	820	1.0E+03	1.0E+10	8.922674E-02	8.753142E-01	7.475623E+01	3.753369E+01	6.774810E+01
ER166	68	166	0	102	823	1.0E+03	1.0E+10	1.431152E-01	2.983558E-01	1.481533E+01	1.954315E+01	3.527527E+01
ER167	68	167	0	102	824	1.0E+03	1.0E+10	6.106636E-02	8.024943E-01	1.590069E+02	1.101003E+03	1.987304E+03

NOTE THAT THE EFFECTIVE THERMAL CROSS SECTION IS THE GROUP 4 CROSS SECTION DIVIDED BY SIGMA(1/V),
WHERE SIGMA(1/V) IS THE GROUP 4 VALUE OF A 1/V CROSS SECTION EQUAL TO 1 BARN AT 2200 M/S (.554018)

Section 5

REDUCED CHAIN STRUCTURE

In many cases, e.g., in spatial depletion calculations, it is desirable only to describe the temporal nature of the aggregate macroscopic absorption buildup in fission products. Here the computational times and details of data management associated with the 84-chain structure would be excessive. We have thus isolated 27 nuclides most responsible for parasitic neutron absorption, including transient effects. These nuclides were combined in 11 linear chains to form a reduced chain structure and data set; subsequent calculations with this data set were compared with those using the 84-chain data set. The difference between results allowed the definition of an additional chain of four fictitious nuclides to accurately describe the balance of macroscopic absorption. The resulting 12-chain structure is shown in Fig. 5.

The 4 fictitious nuclides of the 12th chain are weakly coupled, each having a cross-section value of 1 barn in only 1 group, zero in the remaining 3. Yield fractions were thus chosen such that XXXX1, for example, accurately describes the accumulation of macroscopic absorption in group 1 that is not described by the other 11 chains. The product of a fictitious nuclide's effective fission yield and 1 barn cross section is approximately equal to its associated barns/fission cross section, the difference in 84- and 11-chain values. This value is not constant with time; the value at 20 000 hours of operation was used and, as a result, 84- and 12-chain results are nearly identical at this time.

Cross-section values used for the non-fictitious nuclides of the first 11 chains are identical to those used in the 84-chain structure. Because of the omission of many nuclides, however, the effective fission-yield fractions associated with the nuclides of the 12-chain structure, described in Table 5, are unique to this data set.

Comparison calculations with the 84- and 12-chain data sets show excellent agreement in problems involving fission yields for thermal and fast fission. However, the 12-chain data set errs as much as 20% in reproducing the macroscopic absorption due to fission products resulting from 14-MeV fission as calculated with the 84-chain data set. This disagreement for 14-MeV fission

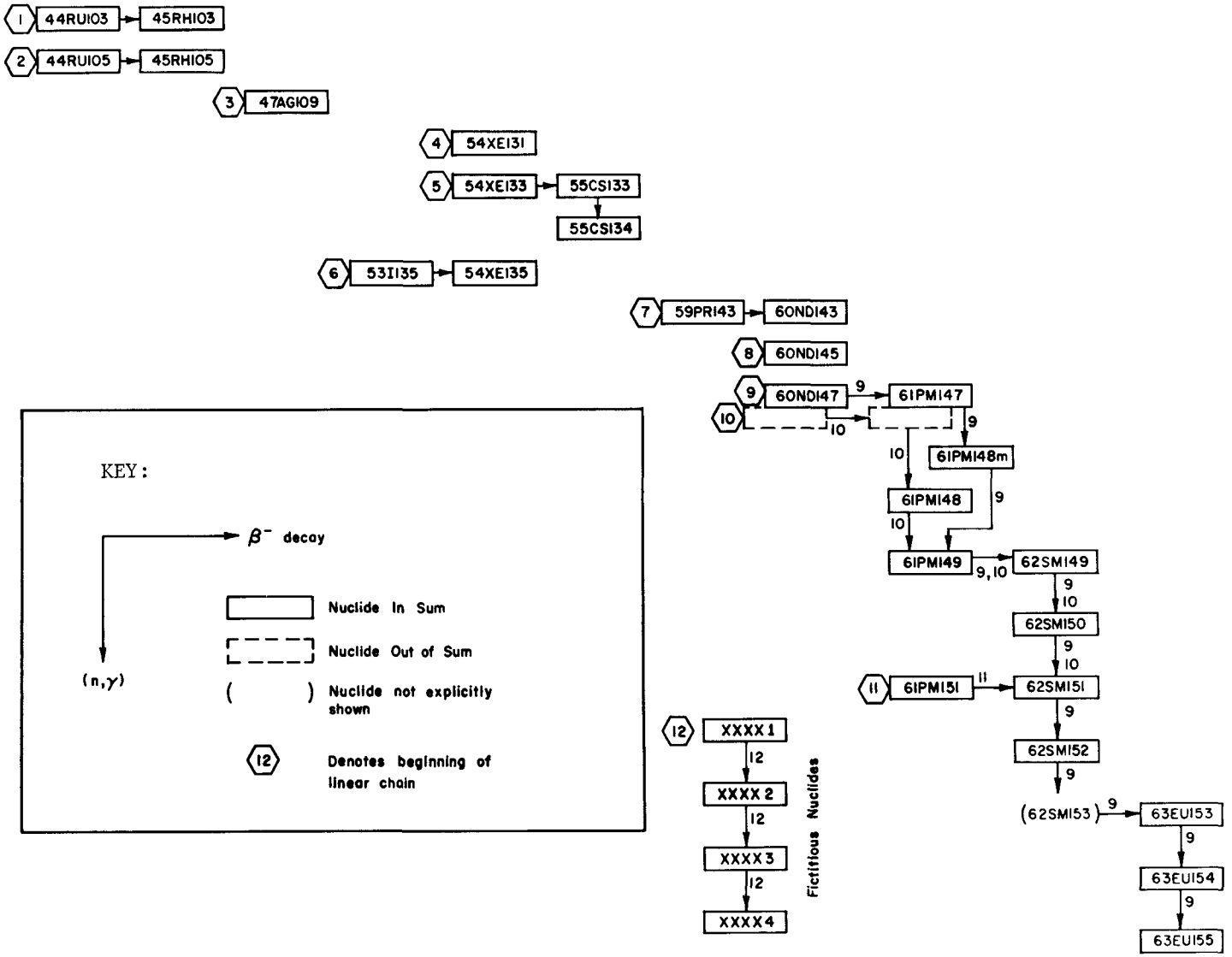

Fig. 5. EPRI-CINDER absorption-decay reduced chain structure.

TABLE 5

DESCRIPTION OF YIELDS 12-CHAIN STRUCTURE

NOTATION----

DY(Z,A,S)=DIRECT YIELD TO NUCLIDE WITH MASS A, CHARGE Z AND STATE S, WHERE 0=GROUND STATE AND 1=METASTABLE STATE

DH(Z,A,S)=DIRECT YIELD TO NUCLIDE WITH MASS A, CHARGE Z AND STATE S, PLUS THE DIRECT YIELD TO EACH NUCLIDE OF THIS MASS WITH HIGHER Z. THE HIGHER-Z ISOBARS ARE TREATED AS IF TO DECAY (B+ OR EC) INSTANTANEOUSLY

CY(Z,A) =CUMULATIVE YIELD, SUM OF DIRECT YIELDS TO NUCLEI OF MASS A AND CHARGE Z OR LESS. LOW-Z ISOBARS ARE TREATED AS IF TO DECAY (B-,IT) INSTANTANEOUSLY.

TY(A) =TOTAL MASS YIELD, THE SUM OF DIRECT YIELDS TO ALL NUCLEI OF MASS A

NUCLIDE	Z	A	S	YIELD DESCRIPTION
RU103	44	103	0	1.000*CY(44,103)
RU105	44	105	0	1.000*CY(44,105)
RH103	45	103	0	1.000*DY(45,103,0) +1.000*DH(45,103,1)
RH105	45	105	0	1.000*DY(45,105,0) +1.000*DY(45,105,1)
AG109	47	109	0	1.000*TY(109)
I135	53	135	0	1.000*CY(53,135)
XE131	54	131	0	1.000*TY(131)
XE133	54	133	0	1.000*CY(54,133)

NUCLIDE	Z	A	S	YIELD DESCRIPTION
XE135	54	135	0	1.000*DY(54,135,0) +1.000*DY(54,135,1)
CS133	55	133	0	1.000*DH(55,133,0)
CS134	55	134	0	1.000*DY(55,134,0) +1.000*DY(55,134,1)
PR143	59	143	0	1.000*CY(59,143)
ND143	60	143	0	1.000*DH(60,143,0)
ND145	60	145	0	1.000*TY(145)
ND147	60	147	0	1.000*CY(60,147)
PM147	61	147	0	1.000*DY(61,147,0)
PM148	61	148	0	1.000*DY(61,148,0)
PM148M	61	148	1	1.000*DY(61,148,1)
PM149	61	149	0	1.000*CY(61,149)
PM151	61	151	0	1.000*CY(61,151)
SM149	62	149	0	1.000*DH(62,149,0)
SM150	62	150	0	1.000*DY(61,150,0) +1.000*DY(62,150,0)
SM151	62	151	0	1.000*DY(62,151,0)
SM152	62	152	0	1.000*CY(62,152)
EU153	63	153	0	1.000*TY(153)
EU154	63	154	0	1.000*DY(63,154,0)
EU155	63	155	0	1.000*CY(63,155)

XXXX1
XXXX2
XXXX3 FICTITIOUS NUCLIDES RECEIVE APPROPRIATE VALUES, SEE TEXT
XXXX4

energies could be reduced with the addition of one or more fictitious nuclides, each forced to reach equilibrium values at different times. However, such an addition is a needless encumbrance to the thermal reactor calculations for which the 12-chain structure is intended.

Section 6
SAMPLE CALCULATIONS

Code Parameters

Part 2 of this report is a self-contained users manual for EPRI-CINDER; it includes listings of the code and data libraries and instructions on their use. In order to perform some elementary sample calculations, we must first examine some of the code characteristics described in Part 2.

We have defined multigroup fluxes and cross sections in Sec. 2 as follows:

$$\phi^j = \int_{E_{j+1}}^{E_j} \phi(E)dE \quad , \tag{7}$$

$$\sigma^j = \frac{\int_{E_{j+1}}^{E_j} \sigma(E)\phi(E)dE}{\int_{E_{j+1}}^{E_j} \phi(E)dE} \quad , \tag{8}$$

where j denotes energy group with upper bound E_j. The product of these quantities is the reaction rate per unit nuclide concentration. Four-group cross sections are listed in Table 4. The four-group fluxes for the PRS Flux Weighting Function are as follows:

$$\phi^1 = \int_{E_2}^{E_1} \phi(E)dE = 0.237019 \quad n/cm^2\text{-sec} \quad ,$$

$$\phi^2 = \int_{E_3}^{E_2} \phi(E)dE = 0.375805 \quad n/cm^2\text{-sec} \quad ,$$

$$\phi^3 = \int_{E_4}^{E_3} \phi(E)dE = 0.286382 \quad n/cm^2\text{-sec} \quad ,$$

$$\phi^4 = \int_{E_5}^{E_4} \phi(E)dE = 0.160593 \quad n/cm^2\text{-sec} \quad . \qquad (9)$$

Fluxes for groups 1-3 are input to EPRI-CINDER as ratios to the thermal (4th) group flux:

$$\phi^1/\phi^4 = 1.475899$$

$$\phi^2/\phi^4 = 2.340108$$

$$\phi^3/\phi^4 = 1.783278 \quad . \qquad (10)$$

The thermal group cross section value used in the EPRI-CINDER data sets is the effective thermal cross section, described in Sec. 4 and more completely in Sec. 1 of Part 2 of this report. The effective thermal cross section is defined as follows:

$$\sigma^4_{eff} = \frac{\sigma^4}{\langle\sigma_{1/v}\rangle} \quad , \qquad (11)$$

where $\langle\sigma_{1/v}\rangle$ is the thermal-group flux-weighted average of a cross section equal to unity at 2200 m/s and having a 1/v dependence. Thus, $\langle\sigma_{1/v}\rangle$ is defined by

$$\langle\sigma_{1/v}\rangle = \frac{\int_{E_5}^{E_4} \sqrt{\frac{.0253}{E}}\ \phi(E)dE}{\int_{E_5}^{E_4} \phi(E)dE} \quad . \tag{12}$$

For the PRS Flux Weighting Function,

$$\langle\sigma_{1/v}\rangle = 0.55402 \quad , \tag{13}$$

and thus

$$\sigma^4_{eff} = \frac{\sigma^4}{0.55402} \quad . \tag{14}$$

The effective thermal group flux must reflect this treatment of the thermal group cross section as follows:

$$\phi^4_{eff} = \langle\sigma_{1/v}\rangle\ \phi^4 \quad . \tag{15}$$

For the PRS Flux Weighting Function,

$$\phi^4_{eff} = 0.55402 \quad \phi^4 = 0.0889717\ \frac{n}{cm^2\text{-sec}} \quad . \tag{16}$$

The group flux ratios we shall input to EPRI-CINDER are then

$$\phi^1/\phi^4_{eff} = 2.66398$$

$$\phi^2/\phi^4_{eff} = 4.22387$$

$$\phi^3/\phi^4_{eff} = 3.21880 \quad . \tag{17}$$

Alternatively, the value of $\langle \sigma_{1/v} \rangle$ could be used as a thermal-spectrum factor; the flux ratios defined by Eq. (10) would then be used. *It is important to note that the EPRI-CINDER libraries do contain effective thermal cross section values. The quantity* $\langle \sigma_{1/v} \rangle$ *must be evaluated for the users' flux and incorporated in the thermal group reaction rate using one of these two alternatives.*

The flux ratios and the thermal flux level may be specified for each time period. Alternatively, the flux ratios and power density (watts/cm^3) during each time step may be specified, from which the corresponding four-group fluxes are determined by the code.* We have specified a constant power density of 100 watts/cm^3 during each of twenty 1000-hour time steps in all sample calculations; using the input flux ratios, flux magnitudes are adjusted for each time step to maintain this power density.

The results of each sample calculation are given in terms of three aggregate quantities evaluated at the end of each time step. These are the effective cross section, resonance integral, and group four cross section defined as follows:

$$\hat{\sigma}_{eff} = \sum_{j=1}^{4} \frac{\phi^j}{\phi^4} \hat{\sigma}_a^j \quad \text{(barns/fission)} \quad , \tag{18}$$

$$\hat{RI} = \int_{E_4}^{E_1} \frac{1}{E} \hat{\sigma}_a(E)dE \simeq 9.088\, \hat{\sigma}_a^3 + 5\hat{\sigma}_a^2 + 2.5\hat{\sigma}_a^1 \quad \text{(barns/fission)} \quad , \tag{19}$$

and $\hat{\sigma}_a^4$, where $\hat{\sigma}_a^j$, expressed in units of barns/fission, is the macroscopic absorption cross section Σ_a^j divided by the total number of fissions per cm^3 that have occured.

The effective cross section $\hat{\sigma}_{eff}$ is a one-group cross section that when multiplied by the thermal group flux will give the same reaction rate as the sum of the group values. This quantity is not to be confused with the effective thermal cross section σ_{eff}^4.

*See Sec. 2, Part 2.

Calculations

Fuel depletion and actinide chains are not a part of the EPRI-CINDER fission-product data sets. However, three fuel depletion chains with appropriate data have been taken from an existing CINDER data set and included in the data set listings of Part 2. The three depletion chains are used in the first two sample calculations below; these describe the fission-product absorption build-up from two different fuel mixtures.

The third and following sample calculations each employ one depletion chain with a single fuel nuclide, corresponding to one of the eight yield sets for thermal and fast neutron fission energies. The fuel nuclide in each of these calculations has the cross-section values of ^{235}U, thus assuring the same depletion and fission rates in order to make fission-product comparisons meaningful.

The sample calculations are summarized in Figs. 6-35. The values of $\hat{\sigma}_{eff}$, $\hat{RI}$, and $\hat{\sigma}_a^4$, as calculated with the 84-chain library, are shown graphically as a function of time during the continuous 20 000 hour period of operation at 100 watts/cm^3. The corresponding values calculated with the 12-chain structure (X) are superimposed.

The intended use of the reduced 12-chain set is their incorporation into spatial depletion codes. The exact duplication of group absorption vs. time is relatively unimportant; rather, it is important that the total absorption over groupd ($=\phi^4\sigma_{eff}$) be correct in order to accurately account for reactivity lifetime. The 12-chain structure not only accurately duplicates the total absorption but also the transient following power changes. Further reduction in the number of chains is possible, but not recommended, particularly because a reduction in chains does not greatly reduce the number of nuclides. However, the minimum number of linear chains is 3 (chains 6, 9, and 12 of Fig. 5). If this is done, the pseudo-nuclide chain (number 12) parameters will have to be recomputed as described at the beginning of this section.

EXAMPLE 1: PWR FUEL

Using 3 depletion chains with a total of 15 depletion linear nuclides

Nuclide	Initial Density (#/b-cm)	Associated Yield Set
^{234}U	5.90×10^{-6}	None
^{235}U	6.30×10^{-4}	^{235}U thermal
^{238}U	2.16×10^{-2}	^{238}U fast
^{239}Pu	0.	^{239}Pu thermal

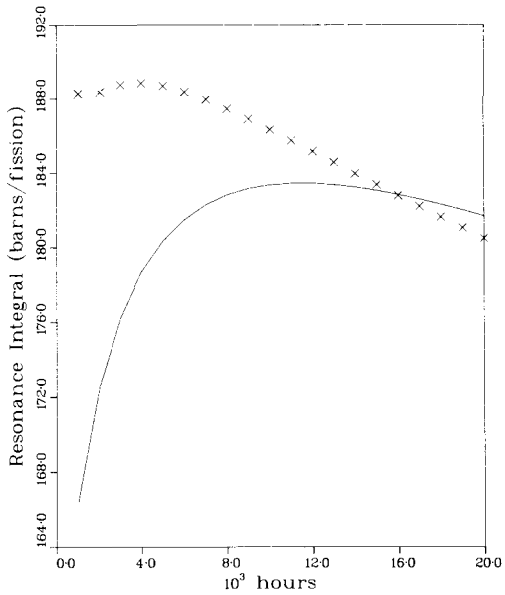

Fig. 6 Resonance integral for PWR fuel example

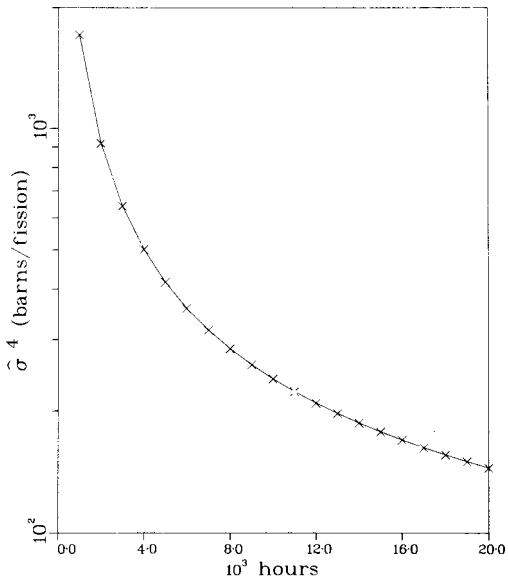

Fig. 7 $\hat{\sigma}^4$ for PWR fuel example

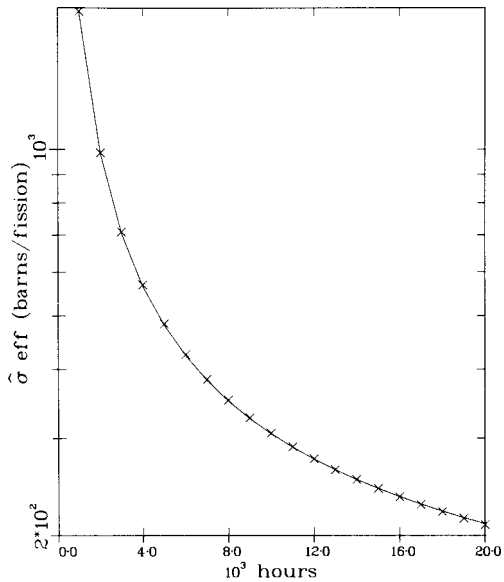

Fig. 8 $\hat{\sigma}$ eff for PWR fuel example

EXAMPLE 2: FIVE FUEL MIX

Using 3 depletion chains with a total of 15 depletion linear nuclides

Nuclide	Initial Density (#/b-cm)	Associated Yield Set
^{232}Th	2.90×10^{-4}	^{232}Th fast
^{233}U	0.	^{233}U thermal
^{234}U	9.0×10^{-8}	None
^{235}U	4.4×10^{-4}	^{235}U thermal
^{238}U	7.2×10^{-7}	^{238}U fast
^{239}Pu	0.	^{239}Pu thermal

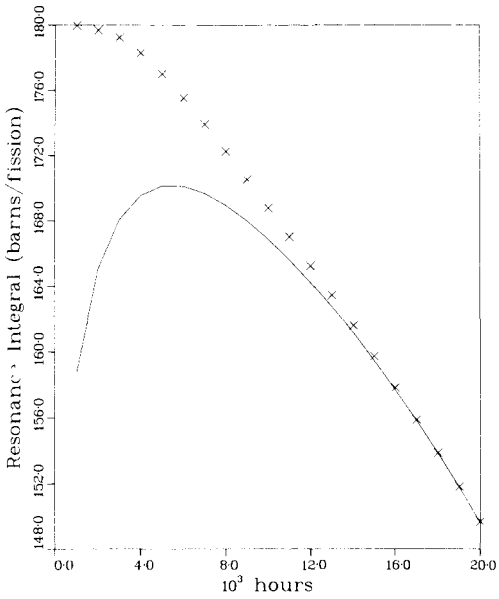

Fig. 9 Resonance integral for five fuel mix example

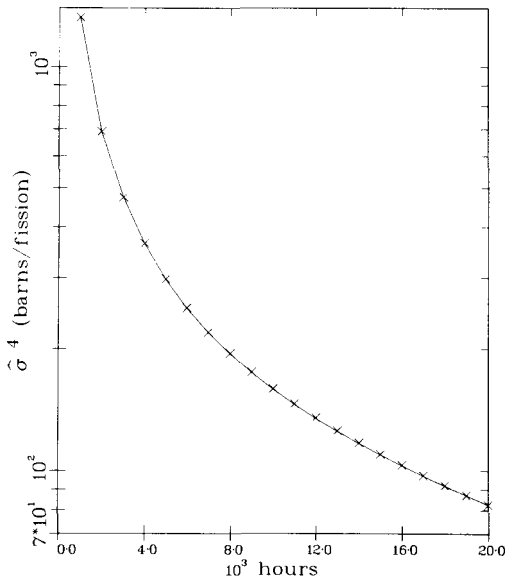

Fig. 10 $\hat{\sigma}^4$ for five fuel mix example

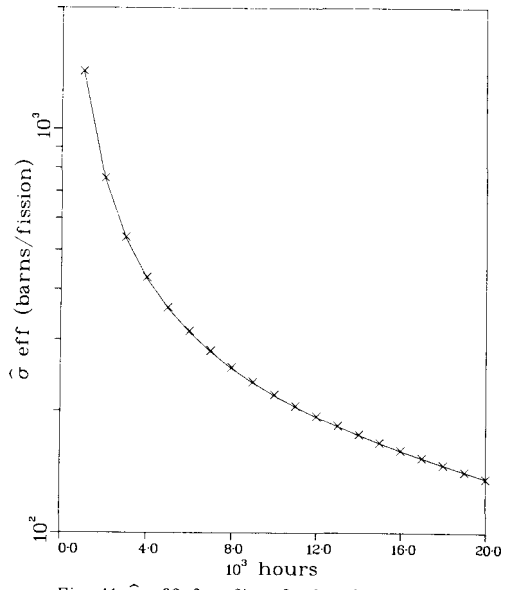

Fig. 11 $\hat{\sigma}$ eff for five fuel mix example

EXAMPLE 3: ^{235}U THERMAL

Using 1 depletion chain with a total of 1 depletion linear nuclide

Nuclide	Initial Density (#/b-cm)	Associated Yield Set
^{235}U	4.6084×10^{-4}	^{235}U thermal

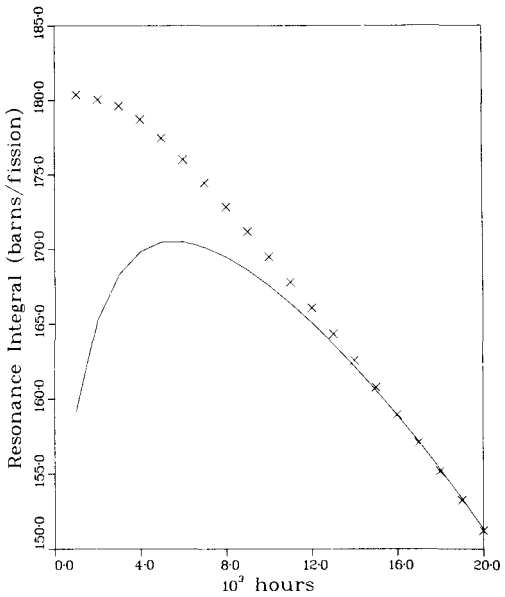

Fig. 12 Resonance integral for U-235 thermal example

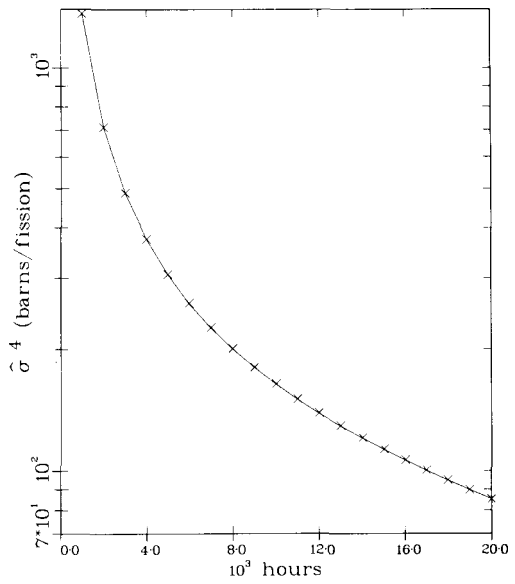

Fig. 13 $\hat{\sigma}^4$ for U-235 thermal example

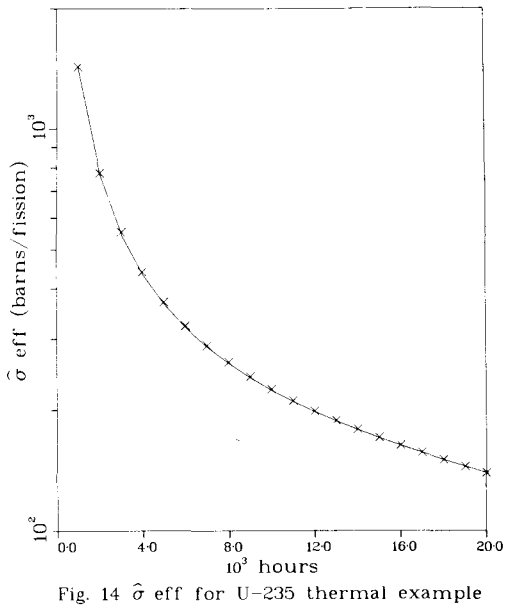

Fig. 14 $\hat{\sigma}$ eff for U-235 thermal example

EXAMPLE 4: ^{238}U FAST

Using 1 depletion chain with a total of 1 depletion linear nuclide

Nuclide	Initial Density (#/b-cm)	Associated Yield Set
^{238}U	4.6084×10^{-4}	^{238}U fast

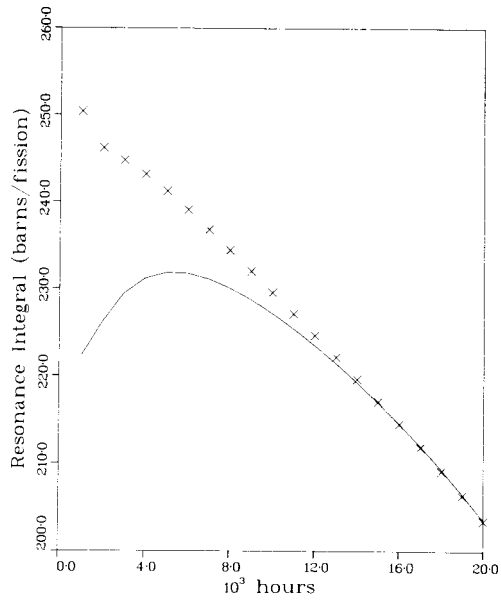

Fig. 15 Resonance integral for U-238 fast example

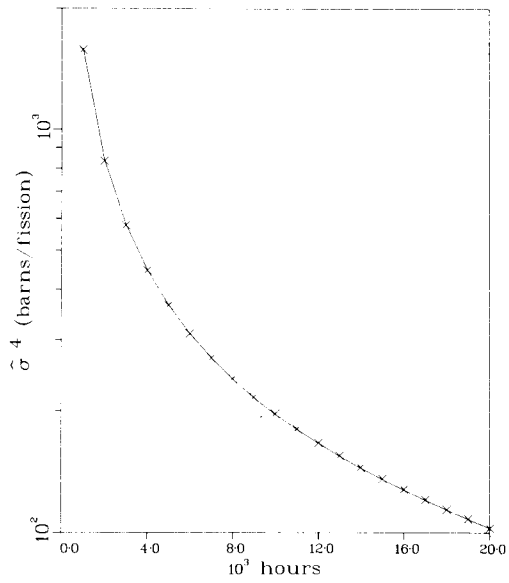

Fig. 16 $\hat{\sigma}$ 4 for U-238 fast example

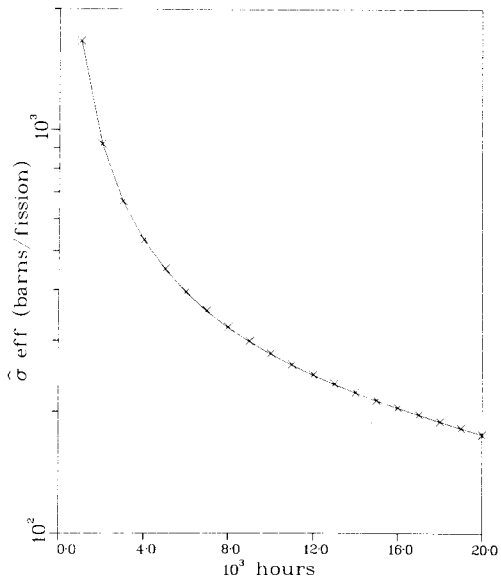

Fig. 17 $\hat{\sigma}$ eff for U-238 fast example

EXAMPLE 5: ^{239}Pu THERMAL

Using 1 depletion chain with a total of 1 depletion lines nuclide

Nuclide	Initial Density (#/b-cm)	Associated Yield Set
^{239}Pu	4.6084×10^{-4}	^{239}Pu thermal

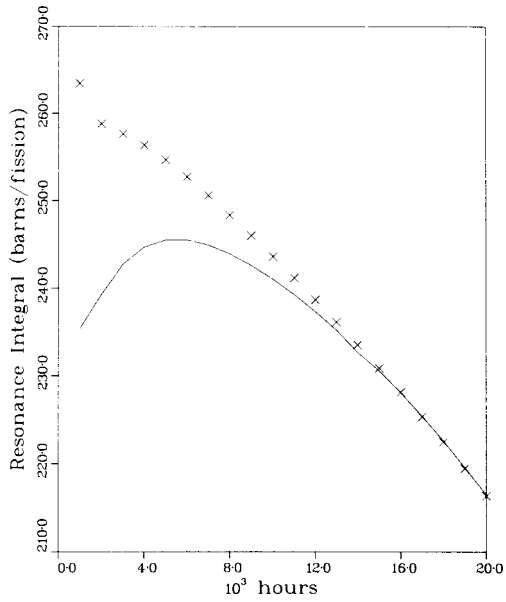

Fig. 18 Resonance integral for PU-239 thermal example

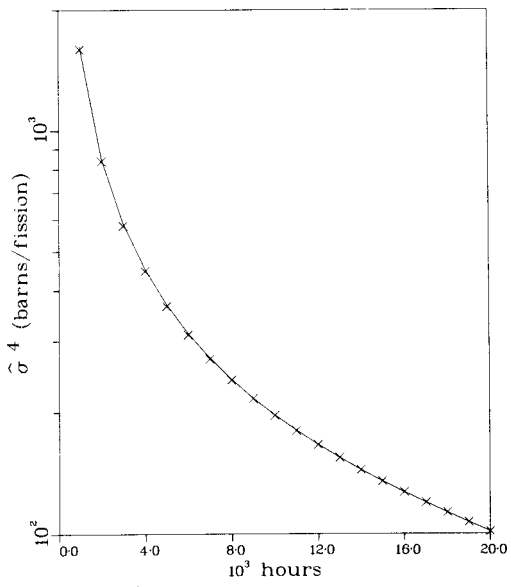

Fig. 19 $\hat{\sigma}^4$ for PU-239 thermal example

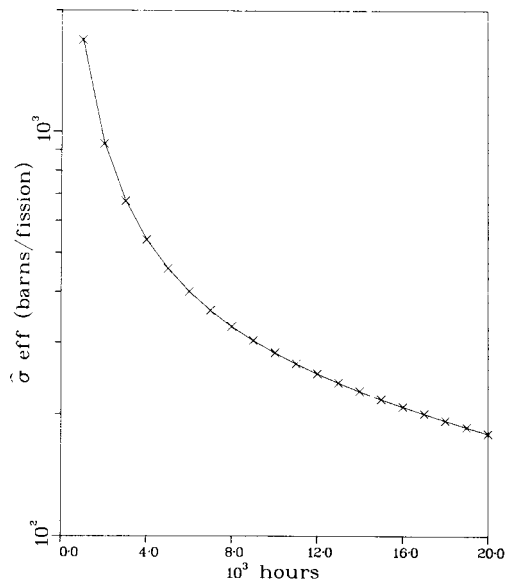

Fig. 20 $\hat{\sigma}$ eff for PU-239 thermal example

EXAMPLE 6: ^{233}U THERMAL

Using 1 depletion chain with a total of 1 depletion linear nuclide

Nuclide	Initial Density (#/b-cm)	Associated Yield Set
^{233}U	4.6084×10^{-4}	^{233}U thermal

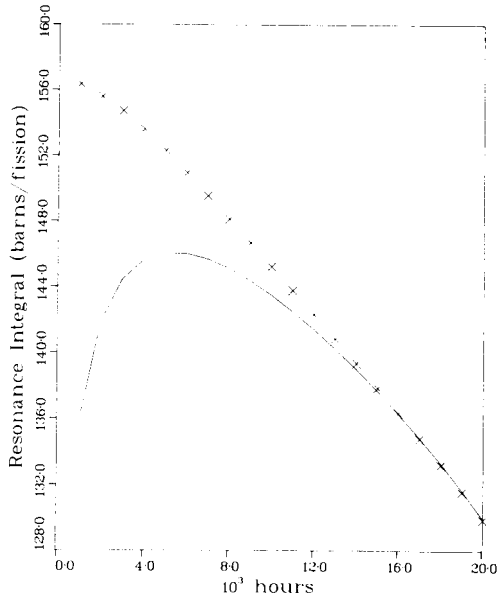

Fig. 21 Resonance integral for U 233 thermal example

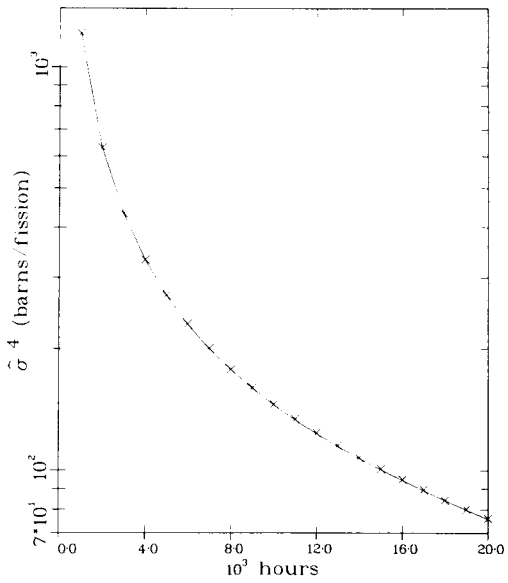

Fig. 22 $\hat{\sigma}^4$ for U-233 thermal example

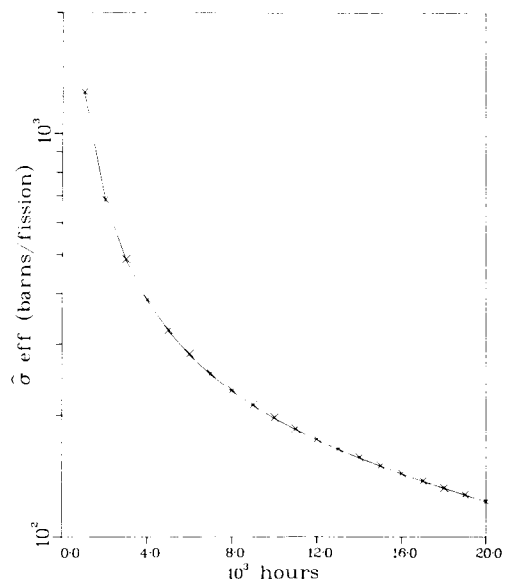

Fig. 23 $\hat{\sigma}$ eff for U-233 thermal example

EXAMPLE 7: ^{232}Th FAST

Using 1 depletion chain with a total of 1 depletion linear nuclide

Nuclide	Initial Density (#/b-cm)	Associated Yield Set
^{232}Th	4.6084×10^{-4}	^{232}Th fast

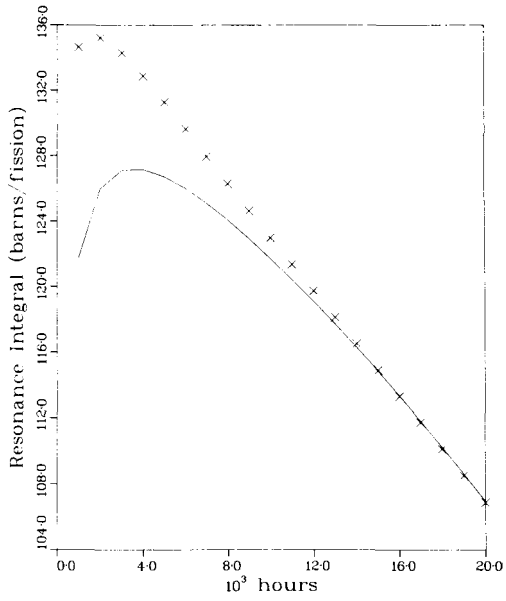

Fig. 24 Resonance integral for TH-232 fast example

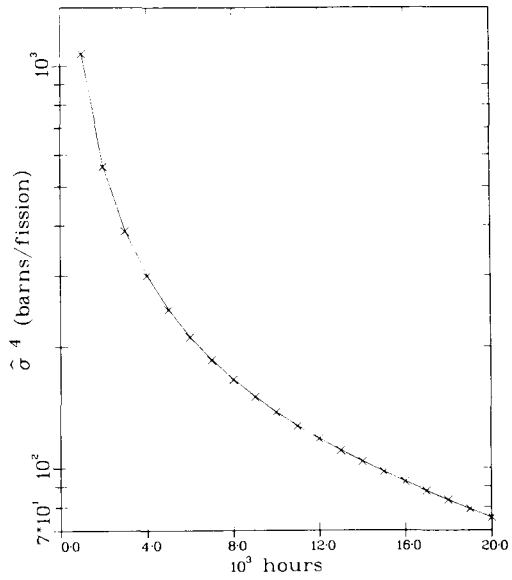

Fig. 25 $\hat{\sigma}^4$ for TH-232 fast example

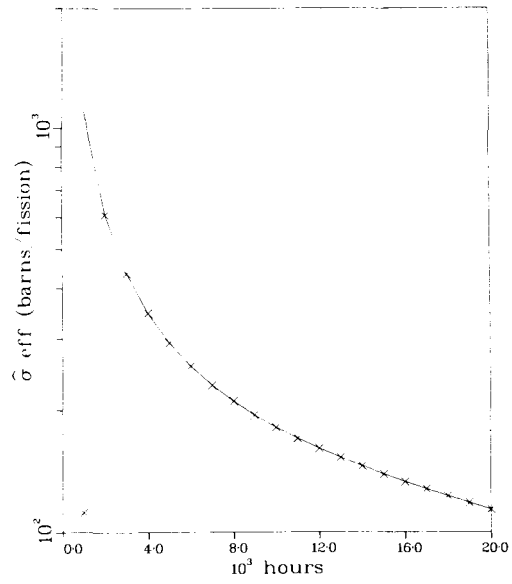

Fig. 26 $\hat{\sigma}$ eff for TH-232 fast example

EXAMPLE 8: ^{235}U FAST

Using 1 depletion chain with a total of 1 depletion linear nuclide

Nuclide	Initial Density (#/b-cm)	Associated Yield Set
^{235}U	4.6084×10^{-4}	^{235}U fast

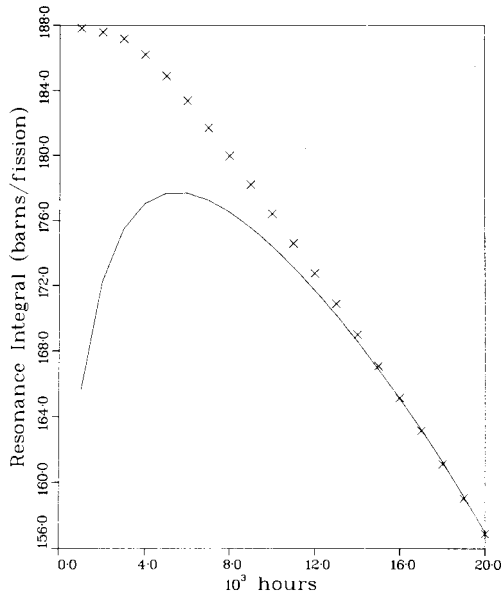

Fig. 27 Resonance integral for U-235 fast example

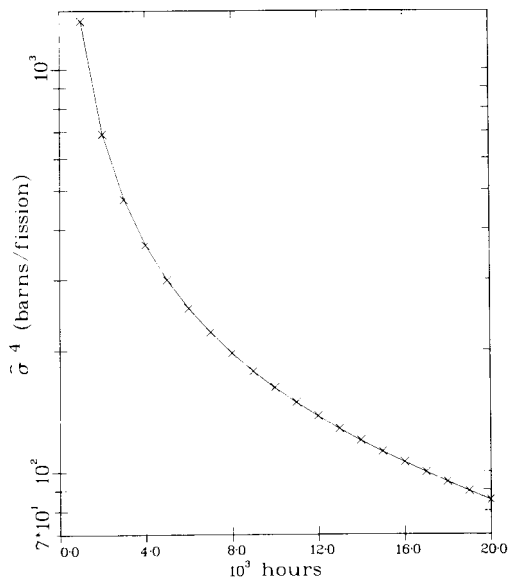

Fig. 28 $\hat{\sigma}^4$ for U-235 fast example

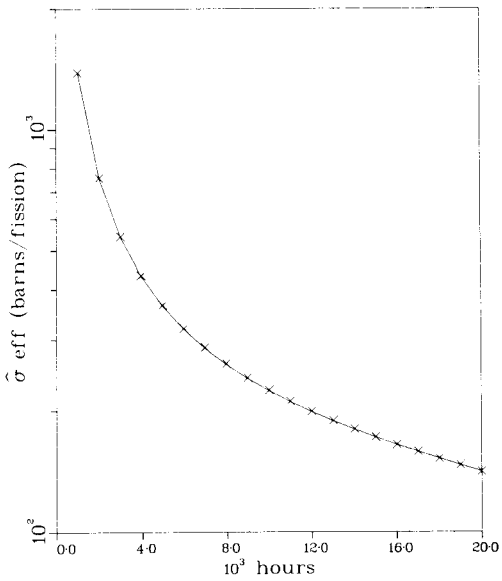

Fig. 29 $\hat{\sigma}$ eff for U-235 fast example

EXAMPLE 9: ^{239}Pu FAST

Using 1 depletion chain with a total of 1 depletion linear nuclide

Nuclide	Initial Density (#/b-cm)	Associated Yield Set
^{239}Pu	4.6084×10^{-4}	^{239}Pu fast

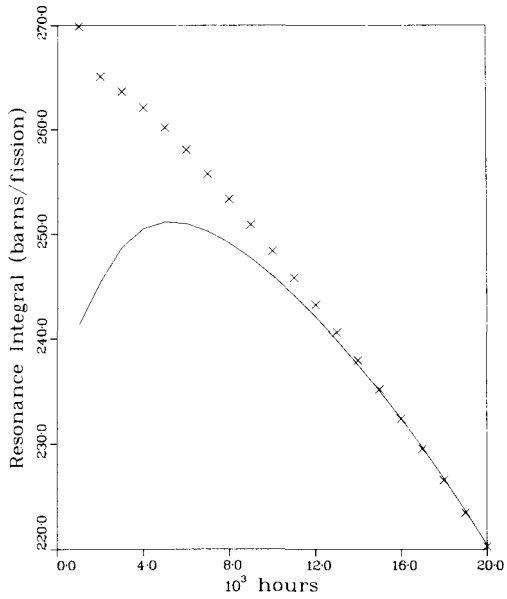

Fig. 30 Resonance integral for PU-239 fast example

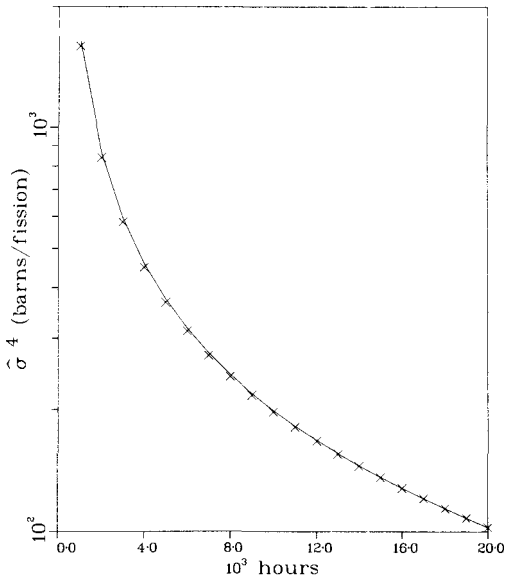

Fig. 31 $\hat{\sigma}^4$ for PU-239 fast example

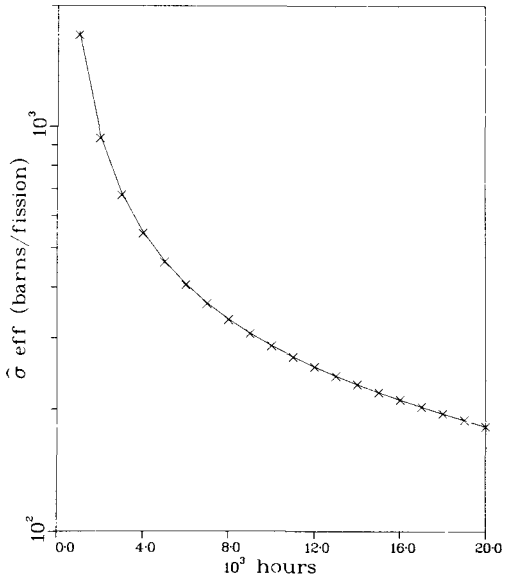

Fig. 32 $\hat{\sigma}$ eff for PU-239 fast example

EXAMPLE 10: ^{241}Pu THERMAL

Using 1 depletion chain with a total of 1 depletion linear nuclide

Nuclide	Initial Density (#/b-cm)	Associated Yield Set
^{241}Pu	4.6084×10^{-4}	^{241}Pu thermal

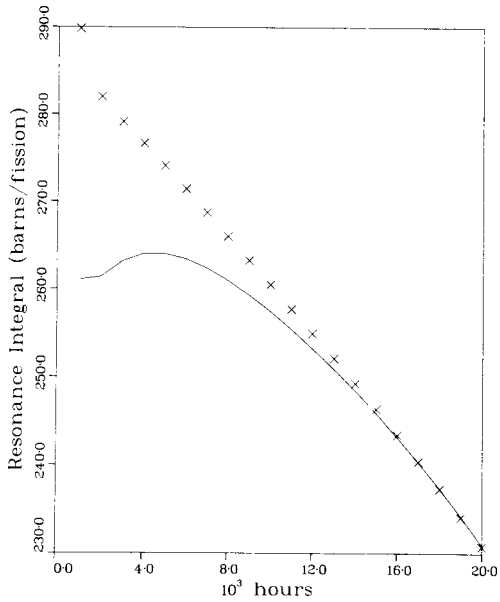

Fig. 33 Resonance integral for PU-241 thermal example

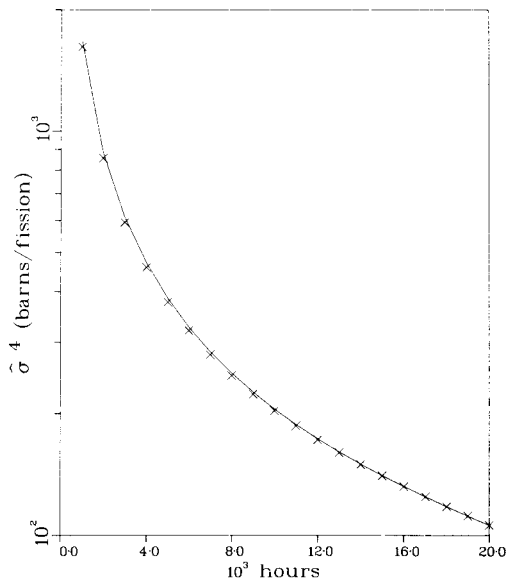

Fig. 34 $\hat{\sigma}^4$ for PU-241 thermal example

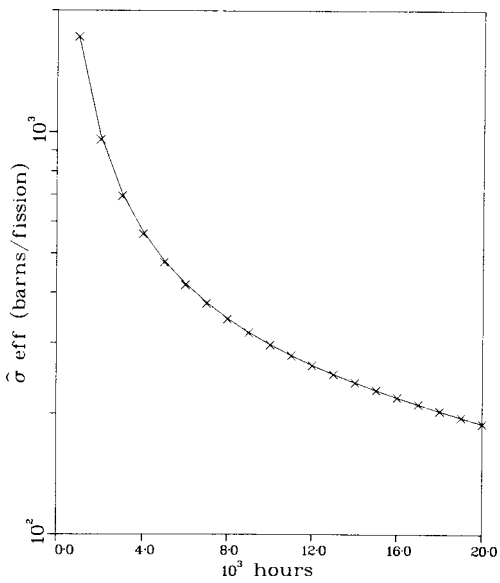

Fig. 35 $\hat{\sigma}$ eff for PU-241 thermal example

Section 7

COMPARISON OF CALCULATED FISSION-PRODUCT ABSORPTION WITH EXPERIMENT

The thermal, epithermal, and total fission-product absorptions calculated by the EPRI-CINDER code were compared with results from ^{233}U irradiation experiments made at the Bettis Atomic Power Laboratory (BAPL) in which there was ~ 95% depletion in the irradiated samples.[11,12] These experiments, which took place over a period of more than 10 years, can be considered to be the best experimental source of information on aggregate fission-product absorption for long-term ^{233}U irradiation in both soft- and hard-neutron spectra.

Although the experiments were made for a variety of ^{233}U and natural thorium samples, the comparison discussed here is restricted to a specific ^{233}U sample (sample 46)* which was irradiated in a relatively hard Materials Testing Reactor (MTR) spectrum to 95% ^{233}U depletion. The neutron spectrum for this sample is closer to actual PWR spectra than unmodified MTR spectra in which the other samples were irradiated. The initial composition of Sample 46 is given in Table 6. The irradiation and cooling history of the sample is shown in Table 7, together with the experimental integrated neutron flux times. The irradiation history of the sample consisted of alternating irradiation periods of approximately three weeks followed by cooling periods of approximately the same duration. During the cooling periods, reactivity measurements of the irradiated sample were made and from these certain quantities related to fission-product thermal and epithermal absorption were calculated. These quantities, to be discussed later, were compared with corresponding quantities calculated with the EPRI-CINDER code and fission-product library for the same irradiation and cooling history as the sample.

The experimental three-group fluxes cover essentially the fast (10 MeV-5530 eV), resonance (5530-0.105 eV), and thermal (0.105-0.0 eV) regions numbered from 1 to 3, respectively. The EPRI-CINDER fission-product library, on the other hand, consists of 4 groups numbered from 1 to 4 and having boundaries at 10 MeV, 8.21 X 10^{-5} eV, 5530, 0.625, and 1.0 X 10^{-5} eV, respectively.

---

*The ^{233}U fission products differ from other fuels only as a result of different yield values, and the comparison is therefore meaningful for all fuels.

TABLE 6

INITIAL ACTINIDE COMPOSITION OF SAMPLE 46

Isotope	Concentration (atoms/barn/cm)
^{232}U	5.4103×10^{-9}
^{233}U	1.0686×10^{-4}
^{234}U	2.5209×10^{-6}
^{235}U	2.2126×10^{-7}
^{236}U	2.2793×10^{-8}
^{238}U	3.9175×10^{-7}

TABLE 7

SAMPLE 46 IRRADIATION AND
COOLING HISTORY AND INTEGRATED FLUX-TIMES

Cycle	Irradiation Time (hrs)	$\phi_1^e t$, 10^{20} n/cm^2	$\phi_2^e t$, 10^{20} n/cm^2	$\phi_3^e t$, 10^{20} n/cm^2	Cooling Time (hrs)
1	442.12	5.50	3.70	1.84	582.25
2	425.75	5.06	3.42	1.61	539.97
3	467.78	5.80	3.90	1.87	589.10
4	406.11	5.10	3.44	1.62	564.35
5	403.05	4.97	3.35	1.61	68.85
6	406.68	4.96	3.34	1.62	65.72
7	422.73	5.51	3.71	1.81	597.83
8	365.39	4.65	3.14	1.52	692.92
9	309.88	3.59	2.42	1.19	50.53
10	429.57	5.32	3.58	1.86	534.17
11	494.38	6.06	4.09	2.15	119.00
12	349.82	4.41	2.97	1.49	647.21
13	351.30	4.37	2.94	1.46	47.50
14	456.28	5.62	3.79	1.95	531.28
15	474.50	5.74	3.86	2.05	90.97
16	269.43	3.16	2.14	1.05	58.08
17	513.30	5.36	3.61	1.84	645.92
18	311.63	3.61	2.43	1.24	71.31
19	397.45	4.67	3.15	1.61	99.82
20	403.86	5.26	3.55	1.73	812.57
21	363.43	4.56	3.06	1.52	1050.35
22	474.47	5.90	3.98	2.09	574.87
23	435.15	5.13	3.46	1.72	530.07
24	405.93	4.77	3.21	1.56	2577.15
25	411.72	5.14	3.47	1.73	20000.00

Since the present comparision is limited to fission-product absorption, we have used the same procedure as BAPL for generating 4-group CINDER fluxes and cross sections for the 3 actinides in the ^{233}U to ^{235}U depletion chain. This procedure is as follows.

Figure 36 shows the CINDER and the BAPL experimental group structures together with the symbols used in the corresponding group cross sections and fluxes. The quantities having a numerical superscript refer to CINDER input quantities to be derived from the BAPL quantities, which have an e superscript.

The group-4 cross section for EPRI-CINDER, σ^4, is set, for input convenience, equal to the effective 2200 m/s cross section, as discussed earlier in this report. The BAPL group-3 cross section, σ_3^e, is calculated as a hardened Maxwellian-averaged thermal cross section with temperature T = 343.2 K and assuming inverse-velocity energy dependence.[11,12]

$$\sigma_3^e = \overline{\sigma}_M = \frac{\int_0^\infty \sigma_0\sqrt{\frac{E_0}{E}}\,\phi_M(E,T)dE}{\int_0^\infty \phi_M(E,T)dE} = \sigma_0\sqrt{\frac{\Pi}{4}}\sqrt{\frac{T_0}{T}} \quad , \tag{20}$$

where the Maxwellian flux distribution $\phi_M(E,T)$ is

$$\phi_M(E,T) = \frac{CONST}{T^{3/2}}\, E\, e^{-E/KT} \quad , \tag{21}$$

k is the Boltzmann constant and σ_0 is the 2200 m/s cross section.

If T_0 = 293.15 and T = 343.2 K, Eq. (20) yields

$$\sigma_3^e = \overline{\sigma_M} = 0.819061\sigma_0 = 0.819061\sigma^4 \quad . \tag{22}$$

Equating reaction rates between 0 and 0.625 eV, one can write:

$$\phi^4\sigma^4 = \phi_3^e\sigma_3^e + \phi_{2A}^e\sigma_{2A}^e \quad . \tag{23}$$

For a 1/E flux in this energy region and through 5530 eV:

$$\phi_{2A}^e = \phi_2^e \frac{\ell n(0.625/0.105)}{\ell n(5530/0.105)} \quad . \tag{24}$$

Assuming inverse-velocity energy dependence of the cross section in the 2A energy region

$$\sigma_{2A}^e = \frac{2\sigma^4\left(\sqrt{0.025261/0.105} - \sqrt{0.025261/0.625}\right)}{\ell n(0.625/0.105)} \quad , \tag{25}$$

we can solve for ϕ^4 from Eqs. (22)-(25)

$$\phi^4 = 0.819061\ \phi_3^e + 0.053248\ \phi_2^e \quad . \tag{26}$$

Also, for an inverse-energy flux dependence in the 0.105 to 5530 eV region:

$$\phi^3 = \phi_2^e \frac{\ell n(5530/0.625)}{\ell n(5530/0.105)} = 0.853924\ \phi_2^e \quad . \tag{27}$$

Inverse-energy flux dependence in the 5530 eV-10 MeV region gives:

$$\phi^1 = \phi_1^e \frac{\ell n(10^7/8.21 \times 10^5)}{\ell n(10^7/5530)} \simeq (1/3)\phi_1^e \quad , \tag{28}$$

and

$$\phi^2 = \phi_1^e \frac{\ell n(8.21 \times 10^5/5530)}{\ell n(10^7/5530)} \simeq (2/3)\phi_1^e \quad . \tag{29}$$

Eqs. (26)-(29) were used for generating CINDER input fluxes from the BAPL experimental fluxes (Table 8); this corresponds to the BAPL analysis[11,12] using a non-ENDF/B data file.

The actinide cross sections for input to CINDER were derived from the BAPL three-group values in a similar fashion. Equating reaction rates between 0 and 5530 eV, one can write:

$$\phi^4\sigma^4 + \phi^3\sigma^3 = \phi_3^e\sigma_3^e + \phi_2^e\sigma_2^e \quad , \tag{30}$$

which together with Eqs. (22) and (26) yields

$$\sigma^3 = 1.196281\ \sigma_2^e - 0.07777146\ \sigma_3^e \quad . \tag{31}$$

For the 5530 eV to 10 MeV region:

$$\phi^1\sigma^1 + \phi^2\sigma^2 = \phi_1^e\sigma_1^e \quad . \tag{32}$$

If a typical MTR spectrum is used for weighting:

$$\sigma^1/\sigma^2 \simeq 2/3 \quad , \tag{33}$$

which together with Eq. (32) gives

$$\sigma^2 = (9/8)\sigma_1^e \quad , \tag{34}$$

and

$$\sigma^1 = (3/4)\sigma_1^e \quad . \tag{35}$$

Eqs. (22), (31), (34), and (35) were used to convert the BAPL 3-group actinide cross sections to the EPRI-CINDER 4-group cross sections (Tables 9 and 10).

TABLE 8

CINDER FLUXES (SAMPLE 46)

Cycle	ϕ^1/ϕ^4	ϕ^2/ϕ^4	ϕ^3/ϕ^4	ϕ^4, Units of 10^{14} n/cm^2/sec
1	1.0758	2.1517	1.8150	1.0707
2	1.1238	2.2477	1.9049	0.9792
3	1.1116	2.2231	1.8744	1.0328
4	1.1258	2.2516	1.9043	1.0329
5	1.1066	2.2132	1.8706	1.0318
6	1.0988	2.1975	1.8555	1.0278
7	1.0932	2.1864	1.8459	1.1040
8	1.0976	2.1952	1.8587	1.0736
9	1.0844	2.1688	1.8331	0.9892
10	1.0346	2.0691	1.7459	1.1084
11	1.0208	2.0417	1.7278	1.1118
12	1.0663	2.1327	1.8009	1.0946
13	1.0771	2.1542	1.8173	1.0693
14	1.0413	2.0827	1.7611	1.0952
15	1.0152	2.0305	1.7121	1.1033
16	1.0815	2.1630	1.8367	1.0041
17	1.0514	2.1028	1.7758	0.9196
18	1.0509	2.1018	1.7740	1.0206
19	1.0473	2.0945	1.7715	1.0389
20	1.0917	2.1835	1.8478	1.1046
21	1.0796	2.1592	1.8168	1.0761
22	1.0223	2.0446	1.7294	1.1263
23	1.0734	2.1469	1.8156	1.0169
24	1.0976	2.1951	1.8523	0.9913
25	1.0697	2.1393	1.8109	1.0807

TABLE 9

BAPL THREE-GROUP ACTINIDE CROSS SECTIONS

Isotope	Absorption Cross Sections (b)			Fission Cross Sections (b)		
	σ^e_{a1}	σ^e_{a2}	σ^e_{a3}	σ^e_{f1}	σ^e_{f2}	σ^e_{f3}
^{233}U	2.2930	114.09	489.67	2.1530	96.80	450.22
^{234}U	1.0963	62.60	86.61	0.7847	0.00	0.00
^{235}U	1.9354	67.24	565.00	1.6136	49.48	483.00

TABLE 10

DERIVED CINDER ACTINIDE CROSS SECTIONS

Isotope	Absorption Cross Sections (b)				Fission Cross Sections (b)			
	σ^1_a	σ^2_a	σ^3_a	σ^4_a	σ^1_f	σ^2_f	σ^3_f	σ^4_f
^{233}U	1.7198	2.5796	98.4013	597.8431	1.6148	2.4221	80.7857	649.6782
^{234}U	0.8222	1.2333	68.1514	105.7430	0.5885	0.8828	0.0000	0.0000
^{235}U	1.4516	2.1773	36.4995	689.8143	1.2102	1.8153	21.6272	589.6997

The fission product absorption quantities for which comparison between the BAPL experiment and the EPRI-CINDER calculations is made are[11,12]

1. The 2200 m/s absorption cross section, σ^e_{2200}:

$$\sigma^e_{2200} = 1.141\ \sigma^e_{a3} \quad . \tag{36}$$

2. The 0.105 to 5530 eV resonance cross section, I^e:

$$I^e = 10.74\ \sigma^e_{a2} + 0.0556\ \sigma^e_{a3} \quad . \tag{37}$$

3. An "effective" cross section, σ^e_{eff}:

$$\sigma^e_{eff} = \sigma^e_{2200} + 0.1123\ I^e(\phi^e_2/\phi^e_3) \quad . \tag{38}$$

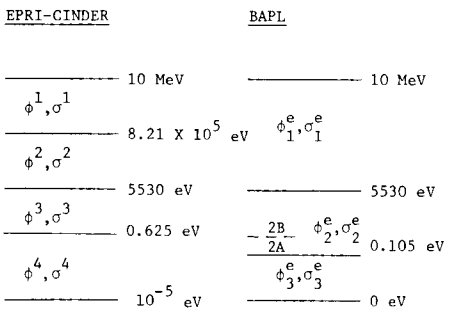

Fig. 36. EPRI-CINDER Library and BAPL Experimental Energy Structures.

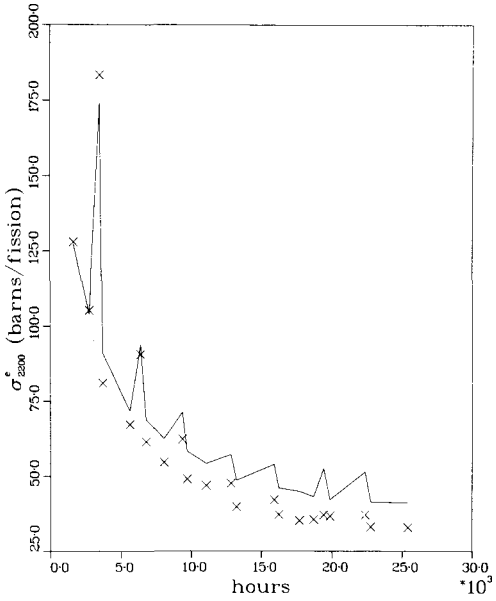

Fig. 37 σ^e_{2200} Comparison. EPRI-CINDER (-) vs. BAPL EXPERIMENTAL (x)

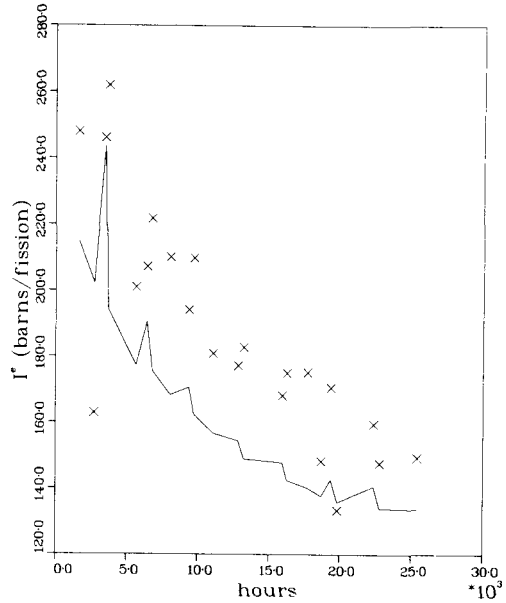

Fig. 38 Resonance cross section I^e comparison EPRI-CINDER (-) vs. BAPL EXPERIMENTAL (x)

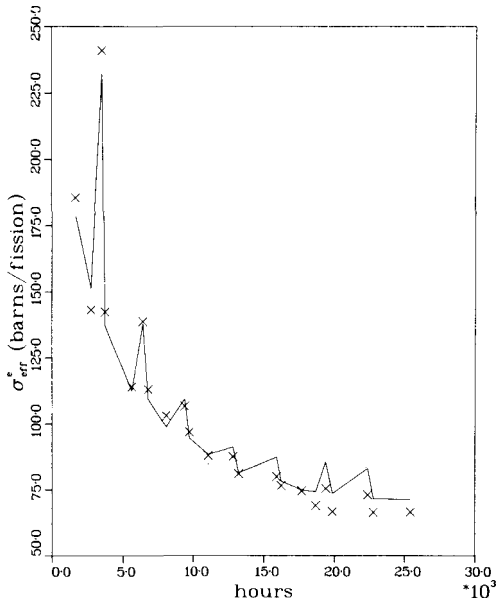

Fig. 39 σ^e_{eff} comparison, EPRI-CINDER (-) vs. BAPL EXPERIMENTAL (x)

Expressing these quantities in terms of EPRI-CINDER fluxes and cross sections we have:

1. $\sigma^e_{2200} = \sigma^4_a$.

2. $I^e = 8.97782\ \sigma^3_a + 0.61742\ \sigma^4_a$. (39)

3. $\sigma^e_{eff} = \sigma^4_a + 0.1123\ I^e \frac{0.95917}{(\phi^4/\phi^3) - 0.06236}$. (40)

The comparison between the EPRI-CINDER results (in terms of σ^e_{2200}, σ^e_{eff}, and I^e) and the BAPL results (both experimental and calculated) is shown in Table 11 and Figs. 37-39. The differences between the EPRI-CINDER and BAPL calculated quantities may reflect the differences between the input libraries. The method used for deriving EPRI-CINDER group fluxes and actinide cross sections from BAPL values is the same as used at BAPL. The BAPL analysis is not entirely valid insofar as it assumes, as shown in the above derivations, inverse-velocity dependent absorption cross sections, hardened Maxwellian thermal fluxes, and inverse-energy epithermal fluxes. It is this method that may be partially responsible for discrepancies between calculated absorption parameters (by both EPRI-CINDER and BAPL) and those derived from the BAPL experimental data. A much better way of obtaining EPRI-CINDER cross sections, for example, is to directly collapse a multigroup cross-section set processed from ENDF/B data to the experimental three-group structure by using as a weighting function the experimental neutron spectrum. Until this is done the most meaningful comparison is that of effective cross sections; these are proportional to the total absorption rate and most closely relate to the fundamental BAPL measurement of reactivity.

It should be noted that the calculated resonance cross section is always significantly lower than the measured value. Because even the hard spectrum case compared here is soft compared to a PWR spectrum, this result implies a significant underprediction of fission-product absorption rates. A more proper comparison than that used by BAPL and repeated here is needed. Such comparison would use ENDF/B-IV data.

TABLE 11

COMPARISON OF FISSION-PRODUCT ABSORPTION (EPRI-CINDER vs BAPL)

Irradiation Cycle	σ^e_{2200} BAPL Exp	σ^e_{2200} BAPL Calc	σ^e_{2200} EPRI-CINDER	I^e BAPL Exp	I^e BAPL Calc	I^e EPRI-CINDER	σ^e_{eff} BAPL Exp	σ^e_{eff} BAPL Calc	σ^e_{eff} EPRI-CINDER
2	128.0	124.7	127.40	248.1	196.4	214.84	185.6	170.3	178.65
3	105.2	101.8	104.07	162.9	196.8	202.25	143.2	147.7	151.44
4	183.4	192.1	174.02	246.2	220.8	243.52	241.0	243.8	232.09
4	81.0	90.6	90.92	262.0	195.6	194.11	142.4	136.4	137.21
7	67.2	71.1	71.70	201.0	185.3	177.31	114.1	114.3	112.52
8	90.6	95.5	93.78	207.2	193.3	190.48	138.8	140.5	137.97
8	61.5	67.6	68.78	221.8	184.1	175.53	113.1	110.5	109.50
10	54.6	59.7	62.43	210.1	177.8	168.30	103.1	100.7	98.80
12	62.3	69.2	71.32	194.1	176.4	170.57	106.7	109.5	109.50
12	49.0	56.6	58.24	209.8	170.9	162.45	96.9	95.6	94.60
14	46.9	52.2	54.23	180.9	164.6	156.72	88.0	89.7	88.44
17	47.6	52.3	57.20	177.2	158.8	154.45	87.6	88.2	91.22
17	39.8	46.2	48.66	182.8	155.2	148.96	81.1	81.2	81.48
21	42.1	46.9	53.96	168.2	148.0	147.85	80.0	80.3	87.38
21	37.2	42.3	46.09	175.0	144.9	142.52	76.6	75.0	78.31
22	35.2	40.6	44.94	175.2	141.6	140.24	74.6	72.5	74.93
23	35.6	38.1	43.17	148.3	138.7	137.75	69.0	69.3	74.29
24	37.1	43.1	52.57	170.6	138.9	142.71	75.5	74.4	85.54
24	36.7	38.0	42.22	133.4	136.0	135.86	66.7	68.6	73.62
25	37.1	41.5	51.43	159.6	135.8	140.68	73.1	72.1	83.12
25	33.1	36.7	41.44	147.7	133.1	134.01	66.4	66.7	71.62
25	32.9	36.2	41.15	149.4	132.4	133.68	66.5	66.0	71.26

REFERENCES

1. T. R. England, "CINDER -- A One-Point Depletion and Fission Product Program," Westinghouse Electric Corporation report WAPD-TM-334 (1962, Rev. 1964).

2. T. R. England, R. Wilczynski, and N. L. Whittemore, "CINDER-7: An Interim Users Report," Los Alamos Scientific Laboratory report LA-5885-MS (1975).

3. T. R. England, "Time-Dependent Fission-Product Thermal and Resonance Absorption Cross Sections," Westinghouse Electric Corporation report WAPD-TM-333 (1962).

4. T. R. England, "Time-Dependent Fission-Product Thermal and Resonance Absorption Cross Sections (Data Revisions and Calculational Extensions)," Westinghouse Electric Corporation report WAPD-TM-333, Addendum No. 1 (1965).

5. T. R. England and R. E. Schenter, "ENDF/B-IV Fission-Product Files: Summary of Major Nuclide Data," Los Alamos Scientific Laboratory report LA-6116-MS (ENDF-223) (1975).

6. R. J. LaBauve and W. B. Wilson, "Proposal to Extend CSEWG Neutron and Photon Multigroup Structures for Wider Applications," Los Alamos Scientific Laboratory report LA-6240-P (1976).

7. R. J. LaBauve, W. B. Wilson, and T. R. England, "PRS Flux Weighting Function," in "Applied Nuclear Data Research and Development," Los Alamos Scientific Laboratory report LA-6472-PR, p. 47 (1976).

8. R. E. MacFarlane and R. M. Boicourt, "NJOY -- A Neutron and Photon Cross-Section Processing System," Trans. Am. Nucl. Soc. 22, 720 (1975).

9. R. J. LaBauve, C. R. Weisbin, R. E. Seamon, M. E. Battat, D. R. Harris, P. G. Young, and M. M. Klein, "PENDF: A Library of Nuclear Data for Monte Carlo Calculations Derived from Data in the ENDF/B Format," Los Alamos Scientific Laboratory report LA-5687 (1974).

10. W. B. Wilson, private communication regarding unpublished codes for the CDC-7600 (CROS).

11. S. B. Gunst et al., "Measured and Calculated Fission-Product Poisoning in Neutron-Irradiated Uranium-233," Nucl. Sci. Eng. 58, 387 (1975).

12. S. B. Gunst et al., "Measurements and Calculations of Heavy Isotopes in Irradiated Fuels and of U-233 Fission-Product Poisoning (LWBR Development Program)," Bettis Atomic Power Laboratory report WAPD-TM-1182 (1974).